https://doi.org/10.1016/j.triboint.2019.05.016

A study of brake contact pairs under different friction conditions with respect to characteristics of brake pad surfaces

L. Wei, Y.S. Choy*, C.S. Cheung

Department of Mechanical Engineering, The Hong Kong Polytechnic University, Hung Hom, Kowloon, Hong Kong

*Corresponding author.

Tel: +852 2766 7813

Email: mmyschoy@polyu.edu.hk

Abstract

In the present study, influences of friction conditions on friction and wear behaviors, as well as characteristics of brake pad surfaces were investigated. Low metallic (LM), semi metallic (SM) and non-asbestos organic (NAO) brake pads sliding against an iron disc were tested using a pin-on-disc tribometer. Results show that the friction coefficient and specific wear rate decrease with increasing contact pressure and sliding velocity. For the morphology of brake pad surface, friction layers are large with few cracks on surfaces of SM and LM brake pads. While for NAO brake pad, friction layers have a comparatively slender and irregular shape. From fractal analysis, the fractal dimension of brake pad surface is in the range of 2.38-2.84 for all brake pads.

Key words: Disc brake; Pin-on-disc; Friction and wear; fractal dimension

Nomenclature

ANOVA	Analysis of variance
BSE	Backscatter electron
COF	coefficient of friction
EDXS	energy-dispersive X-ray spectroscopy
LM	low metallic
NAO	non-asbestos organic
SEM	scanning electron microscopy
SI	supplementary information
SM	semi metallic
XRD	X-ray diffraction
XRF	X-ray fluorescence spectroscopy

1. Introduction

Disc brakes are used to slow down or stop vehicles and trains through pushing brake pads against a brake disc. Performances of disc brakes are determined by the friction and wear process between the brake pad and brake disc which are made of friction materials and grey cast iron respectively. Brake pads contain more than 30 ingredients which can be categorized as binder, reinforcements, fillers and frictional additives [1, 2]. Moreover, brake pads can be classified into three types: low metallic (LM), semi metallic (SM) and non-asbestos organic (NAO) brake pads according to different contents of ingredients. As described in a previous study [3], LM brake pads have a high friction and good braking capacity at high temperature, but have a high wear rate. SM brake pads have a low wear rate but cause high braking noise. NAO brake pads have a low wear rate and brake noise, but they lose braking capacity at high temperature.

Researchers have proved that the wear process is characterized by the formation and disruption of friction layers formed on the contact surfaces of pad and disc [4-6]. Friction layers consist of primary and secondary plateaus [7, 8]. Primary plateaus are formed by hard components, including metal and ceramic fibers, which protrude from the surface. These components had higher hardness than pearlitic grey cast iron [9]. Secondary plateaus are made by compacted wear debris which can move in channels between pad and disc and stack up against the primary plateaus. These wear debris consist of copper, graphite, iron oxides and some other soft components [6, 8]. Previous studies have found that small wear particles, such as copper, can form well compacted secondary plateaus leading to a smooth and stable coefficient of friction (COF). In contrast, less compacted secondary plateaus result in unstable evolution of COF [8]. Secondary plateaus could be classified into type I, with the support of primary plateaus, and type II, without support of primary plateaus [10]. Österle and Urban [11] found the thickness of friction layer was 100 nm and its surface was

covered by a thin film of metal sulphides and graphite which could help to fix wear particles. Alemani et al. [2] investigated characteristics of the friction layer of a LM brake pad under three contact loads and reported iron and copper were major elements of secondary plateaus and iron oxides formed a very thin layer on the surface of secondary plateaus. Federici et al. [6] found the primary plateaus of NAO brake pad consisted of large ceramic particles, such as ZrO_2 and Mg-K-silicate particles. From the literature review, little attention is paid on investigating the change of friction layer of the brake pads when the contact load and sliding velocity are varied. Moreover, most studies related to the characteristics of friction layers were conducted using LM and NAO brake pads, while for SM brake pads with 30-65% of metal content [12, 13], properties of friction layers have not been studied in depth.

Fractal geometry has been introduced to describe the morphology of contact surfaces in tribology because of the self-affinity (a small part can be considered as a reduced-scale image of the whole) of contact surfaces [14-16]. Moreover, fractal properties of contact surfaces can be characterized by a non-integer dimension, called fractal dimension, which value is independent of the resolution of measuring instrument [17]. Yan and Komvopoulos [18] investigated the normal contact of elastic-plastic rough surfaces using three-dimensional fractal geometry and obtained the relationships between total contact force and real contact area in terms of the mean surface separation distance, fractal diameters and material properties. Zhu et al. [19] investigated contacts between two carbon steels with hardness of HRC 30 and HRC 24 and between a carbon steel with hardness of HRC 30 and Cu-Zn alloy under the contact pressure of 0.56 MPa and sliding velocity of 0.55 m/s during running-in stage. They reported fractal dimensions of surface profiles ranging from 1.11 to 1.20 for the worn surface of steel in steel-steel contact and 1.10 to 1.29 for the worn surface of Cu-Zn alloy in steel-Cu-Zn alloy contact at different friction times. Wu et al. [20] investigated the contact between GCr15 steel and C45 steel under different contact pressures and sliding velocities and reported that the fractal dimensions of profiles for

worn surfaces of GCr15 steel were in the range of 1.83-1.90. Contact surfaces on brake pads should also be consider as a self-affine fractal, while their fractal dimensions are lack of study.

In the present study, characteristics of brake pad surface, including morphology, fractal dimension, elemental composition and phase composition were investigated using different brake pads sliding against a pearlitic cast iron disc under different friction conditions. The objectives of the present study are (1) to study the influence of contact pressure and sliding velocity on the change of properties of the brake pad surface; (2) to investigate the characteristics of surface of brake pad with high metal content (larger than 30 wt%). To conduct a broader analysis, SM, LM and NAO brake pads were used in present study.

2. Experimental set-up

2.1.Test set-up and characterization techniques

In order to study the friction and wear behaviors of disc brakes, a pin-on-disc tribometer was built up based on the design of Olofsson et al. [21]. It is considered as a reliable equipment for measuring the wear and friction behaviors of brake pad materials sliding against iron disc [1, 2, 8], although it cannot reflect the actual brake condition. Fig. 1 shows the schematic diagram of the tribometer that includes a horizontal rotating disc and a deadweight loaded brake pad sample (pin). Braking tests were conducted at room temperature and humidity. The tribometer runs under steady conditions with constant normal force and constant rotating speed. The friction coefficient was calculated as the measured tangential force divided by the applied normal force. The tangential force was measured by an HBM Z6FC3/20kg load cell with 1 Hz data sampling rate. A K-type thermocouple was inserted in a hole drilled inside the pin body at a distance of 2 mm from the contact surface to estimate the brake pad temperature. The brake pad temperature was recorded every 10 seconds.

Specific wear rate (k_s) was used to evaluate the wear behavior of brake pad sample and it was calculated based on the equation in ref. [1]:

$$k_s = \frac{\Delta m}{\rho \cdot \Delta s \cdot F_N} \quad (1)$$

Where k_s is the specific wear rate in m^2/N; Δm is the mass loss of sample during the test in g as determined by weighing the sample before and after the test; ρ is the density of sample in g/m^3; Δs is the sliding distance in m; F_N is the applied normal force on the sample in N. The sample's mass is measured through a VIBRA analytical balance with an accuracy of 0.01 mg.

Morphologies and elemental compositions of friction layers on brake pad surface were investigated using a scanning electron microscopy (SEM) equipped with an energy-dispersive X-ray spectroscopy (EDXS) system and a backscatter electron (BSE) detector. Before conducting a SEM measurement, the brake pad sample was coated with a thin layer of gold. About 10 measurements were conducted for each brake pad sample to ensure that the results are reliable and repeatable. To further identify the crystalline phases of friction layers, X-ray diffraction (XRD) measurements were conducted with an IPD 3000 diffractometer using Cu-Kα radiation with Ni-filter. Phase composition was determined through a full pattern fitting procedure based on Rietveld's method [22-24]. SEM pictures with low resolution (50×) were used to calculate the fractal dimension of brake pad surface. Areas of contact plateaus were measured and counted by using a commercial picture processing software Image-Pro Plus 6.0. The corresponding SEM pictures were transformed to white-and-black as shown in Fig. S1 of supplementary information (SI). Contact plateaus became white, while the surroundings became black after the segmentation process. The smallest area of contact plateau was about 500 μm^2. White points or areas smaller than 500 μm^2 were considered as noise and neglected in counting.

2.2. Friction materials

The Pin samples were milled from commercial brake pads and machined to a cubic shape with 10±0.2 mm in length and 7-8 mm in thickness. Three types of brake pad including SM, LM and NAO were used in the present study which were bought from a major manufacturer of brake pads in China. The exact ingredients in a brake pad were not known because they are commercial secret. Therefore, an X-ray fluorescence spectroscopy (XRF) was used to measure the elemental composition of each brake pad as shown in Table 1. Since some light elements such as carbon and oxygen cannot be detected by XRF, the sum of element concentrations is not equal to one hundred. BSE-SEM pictures of brake pad samples are shown in Fig. 2. Some components on brake pad surfaces were identified using EDXS point spectra as shown in Fig. S2 of SI. A commercial brake disc with a diameter of 239 mm and a thickness of 9 mm, bought from BOSH and made of pearlitic grey cast iron, was used in this study. Before conducting the experiments, pin samples were cleaned with air and disc was cleaned with ethanol.

2.3. Design of experiments

Braking tests were conducted at three sliding velocities (v) of 1.6 (low speed), 2.8 (medium speed) and 4.9 m/s (high speed) and at three applied loads of 52 (low load), 81 (medium load) and 122 N (high load) which correspond to nominal contact pressures (p) of 0.52, 0.81 and 1.22 MPa respectively. Friction power (P) is used to analyze the relationship between friction/wear results and friction conditions as shown in the equation below [25, 26].

$$P = \mu F_N v \tag{2}$$

Where P is the frictional power in W; μ is the friction coefficient; F_N is the applied normal load in N; v is the sliding velocity in m/s. Frictional power combines the friction force with sliding velocity which represents the work applied on contact

surfaces by the friction force. The wear track on the disc had a mean diameter of 220 mm. Detailed test conditions and frictional powers are listed in Table 2.

The $p \cdot v$ values range from 0.83-5.98 MPa·m/s which are adequate to investigate these materials because in real brake systems $p \cdot v$ values are in the range of 0.3-20 MPa·m/s [27]. If scaled up to the reference vehicle, the sliding velocities correspond to vehicle speeds of 15.2-46.6 km/h. The selected test conditions are appropriate for simulating the light braking process of a vehicle under urban driving conditions which reduces the vehicle speed but do not stop it. The sliding distance was 22050 m in the middle of the wear track for all tests. The duration of each test varied from 75-230 minutes. Friction force and brake pad temperature were recorded during each test. Experiments were repeated three times and average results are shown in the present study. Analysis of variance (ANOVA) for 3^2 factor design using three repetitions was also conduced to compare influences of sliding velocity and contact pressure on experimental results based on the method in Montgomery [28]. Standard errors, as shown in relevant tables and figures, were calculated following the method in Moffat et al. [29].

3. Results

3.1. Friction and wear behavior

Fig. 3 shows the average friction coefficients with standard errors at steady-state stage for all brake pads and Fig. S3 of SI shows the typical variation of friction coefficient with sliding distance at mode 2 test. The 3^2 ANOVA results of friction coefficient are shown in Table S1 of SI. The friction coefficients are in the ranges of 0.38-0.46, 0.37-0.49 and 0.4-0.48 respectively for SM, LM and NAO brake pads. The friction coefficient increased continually from an initial value to a steady-state value after a running-in stage for all the brake pad samples. Moreover, the running-in stages of SM and LM brake pads are shorter than that of NAO brake pad. Similar

184 phenomena were also observed in other test modes.

185 The friction coefficient decreases with increasing contact pressure for all the
186 brake pads. With increasing sliding velocity, the friction coefficient also decreases in
187 most cases. Both contact pressure and sliding velocity have a significant effect on the
188 friction coefficient based on results of ANOVA analysis. In addition, contact pressure
189 has a higher effect on friction coefficient than sliding velocity for LM and NAO brake
190 pads. But for SM brake pad, they have similar effects on friction coefficient. The very
191 low P-values of interaction for all the brake pads indicates that the variation of friction
192 coefficient with sliding velocity and contact pressure is independent of each other.

193 Fig. 4 shows the average brake pad temperatures with standard errors at
194 steady-state stage and Fig. S4 of SI shows the variation of brake pad temperature with
195 sliding distance at mode 6 test. The 3^2 ANOVA results for brake pad temperature are
196 shown in Table S2 of SI. The average brake pad temperatures increase with increasing
197 contact pressure and sliding velocity for all the brake pads. From ANOVA results,
198 both sliding velocity and contact pressure can significantly affect the brake pad
199 temperature. Moreover, there is a significant interaction on the brake pad temperature
200 between the contact pressure and sliding velocity. Sliding velocity has a stronger
201 effect on brake pad temperature than contact pressure. Due to the difference of
202 thermal conductivity among brake pad samples, the brake pad temperature increases
203 in the order of NAO, LM and SM brake pads which is also in line with the metal
204 contents in these brake pads. The brake pad temperature ranges from 45-130 ℃
205 indicating that the degradation of resin did not occur. Thus, the influence of resin
206 degradation on friction and wear behaviors can be neglected.

207 The specific wear rates (k_s) with standard errors are shown in Fig. 5. The 3^2
208 ANOVA results for specific wear rate are shown in Table S3 of SI. The specific wear
209 rates are in the range of 10^{-15} to 10^{-14} m^2/N which are in line with the previous studies
210 [8, 30, 31]. The specific wear rates decrease with increasing the contact pressure for

all the brake pads and the maximum reduction can reach 36%, 75% and 56% for SM, LM and NAO brake pads respectively when comparing results at the sliding velocity of 4.9 m/s. The specific wear rates also decrease with increasing sliding velocity and the maximum reductions are 69%, 57% and 57% for SM, LM and NAO brake pads respectively when comparing results at the contact pressure of 1.22 MPa. Both sliding velocity and contact pressure have a significant effect on specific wear rate based on the ANOVA analysis. Moreover, there is a significant interaction on the specific wear rate between sliding velocity and contact pressure.

3.2. Characteristics of brake pad surface

3.2.1. Morphology of friction layers

The friction layers on the contact surfaces of brake pads after mode 4 test (low load test) and mode 6 test (high load test) are shown in Figs. 6 and 7 respectively. It can be observed that most of the pin surface is covered by widely distributed friction layers with irregular shape. Comparing the friction layers of these two tests, the following two differences are observed. Firstly, high contact pressure results in more compacted secondary plateaus. Many coarse particles can be observed at the edge of the friction layers after mode 4 test as shown in squares with dashed line in Fig. 6. Secondly, some parts of the friction layers were blown off from the bulk material with some cracks on them as shown in circles with dashed line in Fig. 6. In addition, abrasive grooves can be identified on the surfaces of all brake pads as shown in Fig. 7. This phenomenon indicates the effect of third-body abrasion on the wear behavior of brake pads sliding against iron disc. Generally, the SM and LM brake pads have similar morphology of friction layers with properties of large and well compacted. In contrast, friction layers of the NAO brake pads are slender and more irregular in shape.

Typical friction layers on the surfaces of brake pads after mode 7 test (high speed test) are shown in Fig. S5 of SI. Compared with the friction layers on brake pad after

low speed test, there are more and deeper abrasive grooves on the surface of brake pad. With increasing sliding velocity, kinetic energy of wear debris is increased, which enhances the third-body abrasion on the brake pad surface, leading to deeper abrasive grooves.

Widths of friction layers (D), as marked in Fig. 7, are used to describe the size of friction layer. Four different SEM fields of view were randomly selected and photographed to determine the widths of friction layers. About 20 friction layers were measured in each SEM picture. Fig. 8 shows the average widths of friction layers with standard errors. The 3^2 ANOVA results for the width of friction layer are shown in Table S4 of SI. The mean widths of friction layers increase with increasing contact pressure, while decrease with increasing sliding velocity. In addition, the widths of friction layers of NAO brake pad are smaller than those of SM and LM brake pads. From ANOVA analysis, sliding velocity has significant effect on the width of friction layer, while contact pressure cannot significantly affect it. There is no significant interaction on the width of friction layer between sliding velocity and contact pressure.

High resolution SEM pictures of friction layers for the LM brake pad after mode 6 test (high load test) are shown in Fig. 9. High resolution SEM pictures for the SM and NAO brake pads are shown in Fig. S6 of SI. The primary plateaus circled by white dash lines are formed by Fe fibers. The secondary plateaus are made of compacted wear debris which commonly have a larger size than the primary plateaus.

3.2.2 Fractal dimension measurement

The distribution of contact plateaus on the contact surface of a brake pad follows the power-law relationship as shown below [16].

$$N(A > a) \sim a^{-(D_s-1)/2} \quad (3)$$

Where N(A>a) is the total number of contact plateaus with areas larger than a particular area, a; D_s is the fractal dimension of a surface. The lowest value of a is 500 μm^2, corresponding to the smallest contact plateau that can be identified. Typical number-area distributions of contact plateaus after mode 4 test are shown in Fig. 10. It can be observed that the relationship between N(A>a) and a follows the power-law very well with R^2 larger than 0.99. Then, the fractal dimensions can be evaluated through curve fitting for N(A>a) versus a. Detailed results of fractal dimensions are shown in Table 2. The average fractal dimensions with standard deviations for SM, LM and NAO brake pads are 2.61±0.13, 2.58±0.11 and 2.51±0.06 respectively. The SM and LM brake pads have similar values of fractal dimension and standard deviation which are larger than that of the NAO brake pad. But the difference in fractal dimension among SM, LM and NAO brake pads are not significant at 95% confidence level.

3.2.3. Elemental and phase compositions

Fig. 9 shows the EDXS point spectra acquired from the friction layers of LM brake pad surface after mode 6 test. EDXS point spectra of the SM and NAO brake pad surfaces after mode 6 test are shown in Fig. S6 of SI. Some major elements in the friction material are identified. The friction layers are found to be rich in Fe for all the tested brake pads. The LM and SM brake pads have similar elemental compositions for the friction layers.

The metallic elements, including Fe and Cu, were selected to analyze the variation of elemental composition of friction layers with friction conditions. Ten EDXS measurements were conducted for each brake pad samples. Mean element concentrations with standard errors are shown in Fig. 11 and the relevant 3^2 ANOVA results are shown in Tables S6 and S7 of SI.

As shown in Fig. 11a, the mean values of iron concentrations vary from 54-72%, 42-66% and 17-58% for the SM, LM and NAO brake pads respectively. Iron contents

in the friction layers of SM and LM brake pads are similar and they are higher than that in the friction layer of NAO brake pad. In addition, iron concentrations in the friction layers are also much higher than those in the bulk material of brake pads, as shown in Table 1, in most cases. This phenomenon indicates that most of the iron element is produced from the tribo-oxidation and abrasion of iron disc, which is in line with the previous studies [2, 32]. The influences of contact pressure and sliding velocity are complicated. There are no particular trends for the variation of iron concentration with either the contact pressure or the sliding velocity. The average concentrations of copper with standard errors are shown in Fig. 11b. The copper contents range from 4.8-10.3%, 2.8-8.0% and 3.1-13.5% respectively for the SM, LM and NAO brake pads. There are no special trends for the variation of copper concentration with either the sliding velocity or the contact pressure.

Main phase compositions of the friction layers on brake pad surfaces were measured through XRD analysis. Concentrations of the major phases are quantified following the method in ref. [22] and shown in Table 3. Some minor phases, such as tenorite and zinc, are not quantified because their concentrations are less than 1% and cannot be detected in each brake pad sample. There is no special trend for the phase composition with either the sliding velocity or the contact pressure for each brake pad. As shown in Table 3, mass fractions of graphite are in the ranges of 37.0-60.5%, 43.9-62.1% and 34.1-53.4% respectively for SM, LM and NAO brake pads, which are much higher than that of other elements. It can be observed that the concentration of iron oxides measured by the XRD system is much lower than the concentration measured by the EDXS in most cases. Another finding is that the pure copper concentrations in the friction layers are higher than those in the friction materials in most cases.

4. Discussion

The decrease of friction coefficient with increasing contact pressure can be

attributed to the un-proportional increase of contact area on asperities which results in a reduction of local pressure on the asperities and subsequently a lower friction coefficient [33]. The un-proportional increase of contact area on asperities is mainly due to the viscoelastic properties of friction materials [34]. The decrease of friction coefficient with increasing sliding velocity is due to the increment of sliding velocity which reduces the contact time between asperities of brake pad and disc, then reducing the possibility of forming strong junctions by adhesion [35].

Shorter running-in stages of the LM and SM brake pads compared with that of the NAO brake pad can be attributed to higher metal contents in LM and SM brake pads. As shown in Table 1, metal contents in the NAO brake pad (Fe+Cu: 14.97%) are much lower than those in LM (Fe+Cu: 31.61%) and SM brake pads (Fe+Cu: 38.47%). Higher metal content can generate more primary plateaus which provide the majority of friction force and more type I secondary plateaus with good compactness and adhesion strength. Therefore, friction force increases and reaches a steady-state value quickly.

The reduction of specific wear rate with increasing contact pressure is mainly due to the higher contact pressure which improves the compactness of secondary plateaus and subsequently reduces their possibility to be detached. The reduction of specific wear rate with increasing sliding velocity is due to the lower friction coefficient results in the lower shear force on contact plateaus leading to a lower specific wear rate. The relationship between specific wear rate and frictional power is shown in Fig. 12. A good linear relationship is observed for the NAO brake pad and close to linear relationship is observed for the SM brake pad. The fitting parameters are shown in Table S5 of SI. The friction and wear process are determined by adhesion and abrasion between contact surfaces. Adhesion varies with sliding velocity and contact pressure [35] while abrasion is almost independent from contact pressure and sliding velocity [36]. The high values of adjusted R square, as shown in Table S5 of SI, indicate that the wear mechanism for brake pad is mainly determined by the adhesive

wear mechanism.

Different morphologies between SM/LM brake pads and NAO brake pads are due to the lower iron content in the NAO brake pad than that in SM and LM brake pads, as shown in Table 1. Effects of iron on friction layers have been introduced in ref. [37]. With the lack of iron, other hard elements, such as ceramic particles, quartz and Aluminum oxides, can work as primary plateaus. Thus, the different characteristics between steel fibers and these hard particles, including size and shape, result in different shapes of primary and secondary plateaus. Moreover, comparing NAO brake pad with SM and LM brake pads, more type II secondary plateaus with an irregular shape are formed on the brake pad surface because type II secondary plateaus do not have the support of primary plateaus.

Sliding velocity can significantly affect the width of a friction layer. It is mainly because the higher sliding velocity leads to higher kinetic energy of the wear debris which reduces the probability of wear debris being blocked by the primary plateaus and hence reducing the width of friction layer. With increasing contact pressure, the space between the brake pad and disc is reduced. Therefore, more wear debris is blocked by the primary plateaus and larger secondary plateaus are formed. In this mechanism, extension of secondary plateaus is mainly along the sliding direction. For the width of a friction layer, which is orthogonal to the sliding direction, contact pressure cannot significantly affect it. Therefore, contact pressure cannot significantly affect the width of a friction layer.

There is no special trend for the variation of fractal dimension with either the contact pressure or sliding velocity for all the brake pads. On the one hand, increments of sliding velocity and contact pressure lead to a more complicated friction and wear process and subsequently increase the complexity of surface profile which contributes to a higher fractal dimension [20]. On the other hand, contact plateaus with a high slope, corresponding to a high fractal dimension, would be very fragile

and easily damaged by interactions with other objects [38]. Therefore, no special trends are observed for the variation of fractal dimension with either contact pressure or sliding velocity.

Standard deviation of the fractal dimension for the NAO brake pad surface is smaller than those for the SM and LM brake pad surfaces. This smaller standard deviation indicates that the variation of rms slope for the surface of the NAO brake pad is lower than those for the surfaces of SM and LM brake pads. This phenomenon can be attributed to the different wear resistant of contact plateaus on the contact surfaces between SM/LM brake pads and NAO brake pad. High metal contents in SM and LM brake pads can provide many primary plateaus and type I secondary plateaus with high wear resistant on contact surfaces. For SM and LM brake pads, the high wear resistant of contact plateaus reduces their possibility to be cracked, hence contributing to a high fractal dimension [38]. This phenomenon becomes more pronounced in friction conditions with high frictional power, as shown in Fig. S7 of SI, leading to high standard deviations of fractal dimensions for the SM and LM brake pads. For the NAO brake pad, the relatively low wear resistant of contact plateaus on its surface reduces the fractal dimension leading to a lower standard deviation.

Person [38] reported most natural and man-made rough surfaces are three-dimensional fractal surface with a typical dimension ranging from 2-2.3 because when the fractal dimension is larger than 2.3, the surface will be very fragile and damaged easily due to the high average surface slope. But in the present study, all the fractal dimensions are higher than 2.3. This phenomenon may be due to the large difference in hardness between the contact plateaus and surrounding matrix of the brake pad surface. Eriksson and Jacobson [5] reported the hardness of secondary plateaus of NAO brake pad ranges from 0.2-4 GPa through nanoindentation test, while the hardness of surrounding matrix is about 200 MPa through regular microhardness indentation test. The large difference in hardness between the contact plateaus and matrix increases the height variation of surface profile, leading to a high

fractal dimension.

Compared with the iron contents measured with EDXS, the lower iron contents measured with XRD are mainly due to the much smaller penetration depth for X-rays of EDXS system than that for X-rays of XRD system. Iron oxides generated from tribo-oxidation are widely distributed in the friction layers on the brake pad surface. But they form a thin layer and contributes a limited fraction to the total diffraction intensity. Therefore, the mass fraction of iron oxides measured by XRD is much smaller than that measured by EDXS.

The higher copper contents in friction layers compared with that in bulk materials is mainly due to the copper fibers milled into copper particles which are widely dispersed in the friction layer. These copper particles can improve the compactness of the friction layer and reduce its tendency to be broke down into wear debris [39]. Therefore, higher copper content is measured in the friction layers. This phenomenon becomes more pronounced for the NAO brake pad at the sliding velocity of 4.9 m/s or at the contact pressure of 1.22 MPa. As shown in Fig. 11b, the copper contents in the friction layers of NAO brake pad at these heavy friction conditions are significantly higher than those measured at other friction conditions. For NAO brake pad, there are many type II secondary plateaus on the contact surface where wear resistance relies more on copper compared with type I secondary plateaus. Therefore, copper contents in the friction layers of the NAO brake pad after brake tests with high sliding velocity or high contact pressure become very high. For SM and LM brake pads, similar phenomenon cannot be observed due to their high iron contents. Most secondary plateaus of SM and LM brake pads are supported by primary plateaus which reduces their tendency to be broken down.

5. Conclusions

Three types of brake pad were tested by sliding against an iron disc to investigate

427 the influences of sliding velocity and contact pressure on friction and wear behaviors,
428 as well as characteristics of the brake pad surfaces. The following conclusions can be
429 drawn from the present study.

430 1. Friction coefficient and specific wear rate decrease with increasing the contact
431 pressure and sliding velocity. From ANOVA analysis, both contact pressure and
432 sliding velocity have significant effect on these two parameters.

433 2. Friction layers on surfaces of SM and LM brake pads are large with few cracks,
434 while the friction layer on surface of NAO brake pad has comparatively slender
435 and irregulated shape.

436 3. The number-area distribution of contact plateaus follows the power-law very well
437 and fractal dimension of brake pad surface ranges from 2.38-2.84. With different
438 friction conditions, the variation of the fractal dimension for NAO brake pad is
439 smaller than that for SM and LM brake pads.

440 4. There are no particular trends for iron and copper contents and main phase
441 compositions with either the sliding velocity or the contact pressure. Iron oxides
442 are widely dispersed in the friction layer with a shallow depth leading to the
443 different iron concentrations between XRD and EDXS results.

444 Results present a deeper understanding of the role of friction conditions on the
445 morphologies and elemental compositions of the friction layers on brake pad surfaces
446 which helps to understand the variation of composition of airborne wear particles
447 emitted from disc brakes under different friction conditions.

448 Experiments were conducted under constant sliding velocity and contact pressure.
449 But in real friction conditions, some brakes occur in a short time only including the
450 running-in stage. Further study should be conducted in the running-in stage to validate
451 if results obtained under steady-state stage are still correct under running-in stage. In
452 the present study, the brake pad temperature is lower than the critical temperature of

resin degradation (230-475 ℃). Thus, resin degradation is not considered. Future studies should investigate the change of properties of brake pad surface with different friction conditions under the critical temperature that resin degradation occurs.

Acknowledgement

Authors would like to thank Prof. Poon, Chi Sun at the department of civil and environment engineering for the XRF test and also thank The Hong Kong Polytechnic University for the financial support (RUTT).

References

[1] Wahlstrom J, Lyu YZ, Matjeka V, Soderberg A. A pin-on-disc tribometer study of disc brake contact pairs with respect to wear and airborne particle emissions. Wear. 2017;384:124-30.

[2] Alemani M, Gialanella S, Straffelini G, Ciudin R, Olofsson U, Perricone G, et al. Dry sliding of a low steel friction material against cast iron at different loads: Characterization of the friction layer and wear debris. Wear. 2017;376-377:1450-9.

[3] Sanders PG, Xu N, Dalka TM, Maricq MM. Airborne Brake Wear Debris: Size Distributions, Composition, and a Comparison of Dynamometer and Vehicle Tests. Environ Sci Technol. 2003;37:4060-9.

[4] Cho MH, Cho KH, Kim SJ, Kim DH, Jang H. The Role of Transfer Layers on Friction Characteristics in the Sliding Interface between Friction Materials against Gray Iron Brake Disks. Tribol Lett. 2005;20:101-8.

[5] Eriksson M, Jacobson S. Tribological surfaces of organic brake pads. Tribol Int. 2000;33:817-27.

[6] Federici M, Gialanella S, Leonardi M, Perricone G, Straffelini G. A preliminary investigation on the use of the pin-on-disc test to simulate off-brake friction and wear characteristics of friction materials. Wear. 2018;410-411:202-9.

[7] Österle W, Griepentrog M, Gross T, Urban I. Chemical and microstructural changes induced by friction and wear of brakes. Wear. 2001;251:1469-76.

[8] Chandra Verma P, Menapace L, Bonfanti A, Ciudin R, Gialanella S, Straffelini G. Braking pad-disc system: Wear mechanisms and formation of wear fragments. Wear. 2015;322-323:251-8.

[9] Österle W, Prietzel C, Kloß H, Dmitriev AI. On the role of copper in brake friction materials. Tribol Int. 2010;43:2317-26.

[10] Neis PD, Ferreira NF, Fekete G, Matozo LT, Masotti D. Towards a better understanding of the structures existing on the surface of brake pads. Tribol Int. 2017;105:135-47.

[11] Österle W, Urban I. Friction layers and friction films on PMC brake pads. Wear. 2004;257:215-26.

[12] Chan D, Stachowiak GW. Review of automotive brake friction materials. Proceedings of the Institution of Mechanical Engineers, Part D: Journal of Automobile Engineering. 2004;218:953-66.

[13] El-Sonbaty IA, Khashaba UA, Selmy AI, Ali AI. Prediction of surface roughness profiles for milled surfaces using an artificial neural network and fractal geometry approach. J Mater Process Technol. 2008;200:271-8.

[14] Komvopoulos K, Ye N. Three-dimensional contact analysis of elastic-plastic layered media with fractal surface topographies. J Tribol. 2001;123:632-40.

[15] Thomas TR, Rosén BG, Amini N. Fractal characterisation of the anisotropy of rough surfaces. Wear. 1999;232:41-50.

[16] Majumdar A, Bhushan B. Role of Fractal Geometry in Roughness Characterization and Contact Mechanics of Surfaces. J Tribol. 1990;112:205-16.

[17] Mandelbrot B. How long is the coast of britain? Statistical self-similarity and fractional dimension. Science. 1967;156:636-8.

[18] Yan W, Komvopoulos K. Contact analysis of elastic-plastic fractal surfaces. J Appl Phys. 1998;84:3617-24.

[19] Zhu H, Ge S, Huang X, Zhang D, Liu J. Experimental study on the characterization of worn surface topography with characteristic roughness parameter. Wear. 2003;255:309-14.

[20] Wu Z-h, Zhu H, Li G. Research on the relation of fractal dimension of friction coefficient to load and velocity. TRIBOLOGY-BEIJING-. 2007;27:165.

[21] Olofsson U, Olander L, Jansson A. A Study of Airborne Wear Particles Generated From a Sliding Contact. Journal of Tribology-Transactions of the Asme. 2009;131:044503-4.

[22] Verma PC, Alemani M, Gialanella S, Lutterotti L, Olofsson U, Straffelini G. Wear debris from brake system materials: A multi-analytical characterization approach. Tribol Int. 2016;94:249-59.

[23] Lutterotti L, Matthies S, Wenk HR, Schultz AS, Richardson JW. Combined texture and structure analysis of deformed limestone from time-of-flight neutron

520 diffraction spectra. J Appl Phys. 1997;81:594-600.

521 [24] Lutterotti L. Total pattern fitting for the combined size–strain–stress–texture
522 determination in thin film diffraction. Nucl Instrum Methods Phys Res, Sect B.
523 2010;268:334-40.

524 [25] Alemani M, Wahlström J, Olofsson U. On the influence of car brake system
525 parameters on particulate matter emissions. Wear. 2018;396-397:67-74.

526 [26] Bettge D, Starcevic J. Topographic properties of the contact zones of wear
527 surfaces in disc brakes. Wear. 2003;254:195-202.

528 [27] Straffelini G, Maines L. The relationship between wear of semimetallic friction
529 materials and pearlitic cast iron in dry sliding. Wear. 2013;307:75-80.

530 [28] Montgomery DC. Design and analysis of experiments. Eighth ed: John wiley &
531 sons; 2013.

532 [29] Moffat RJ. Describing the uncertainties in experimental results. Exp Therm Fluid
533 Sci. 1988;1:3-17.

534 [30] Wahlström J, Matějka V, Lyu Y, Söderberg A. Contact Pressure and Sliding
535 Velocity Maps of the Friction, Wear and Emission from a Low-Metallic/Cast-Iron
536 Disc Brake Contact Pair. Tribology in Industry. 2017;39.

537 [31] Hong US, Jung SL, Cho KH, Cho MH, Kim SJ, Jang H. Wear mechanism of
538 multiphase friction materials with different phenolic resin matrices. Wear.
539 2009;266:739-44.

540 [32] Kukutschová J, Roubíček V, Malachová K, Pavlíčková Z, Holuša R, Kubačková J,
541 et al. Wear mechanism in automotive brake materials, wear debris and its potential
542 environmental impact. Wear. 2009;267:807-17.

543 [33] Persson BNJ. Sliding friction : physical principles and applications. 2nd ed.. ed.
544 Berlin: Springer; 2000.

545 [34] Bijwe J, Aranganathan N, Sharma S, Dureja N, Kumar R. Nano-abrasives in
546 friction materials-influence on tribological properties. Wear. 2012;296:693-701.

547 [35] Straffelini G. Friction and wear: methodologies for design and control: Springer;
548 2015.

549 [36] Straffelini G, Pellizzari M, Molinari A. Influence of load and temperature on the
550 dry sliding behaviour of Al-based metal-matrix-composites against friction
551 material. Wear. 2004;256:754-63.

552 [37] Eriksson M, Bergman F, Jacobson S. On the nature of tribological contact in
553 automotive brakes. Wear. 2002;252:26-36.

554 [38] Persson BNJ. On the Fractal Dimension of Rough Surfaces. Tribol Lett.

555 2014;54:99-106.

556 [39] Menapace C, Leonardi M, Perricone G, Bortolotti M, Straffelini G, Gialanella S.
557 Pin-on-disc study of brake friction materials with ball-milled nanostructured
558 components. Materials & Design. 2017;115:287-98.

A study of brake contact pairs under different brake conditions with respect to characteristics of brake pad surfaces

L. Wei, Y.S. Choy*, C.S. Cheung
Department of Mechanical Engineering, The Hong Kong Polytechnic University, Hung Hom, Kowloon, Hong Kong

*Corresponding author.
Tel: +852 2766 7813
Email: mmyschoy@polyu.edu.hk

Figures

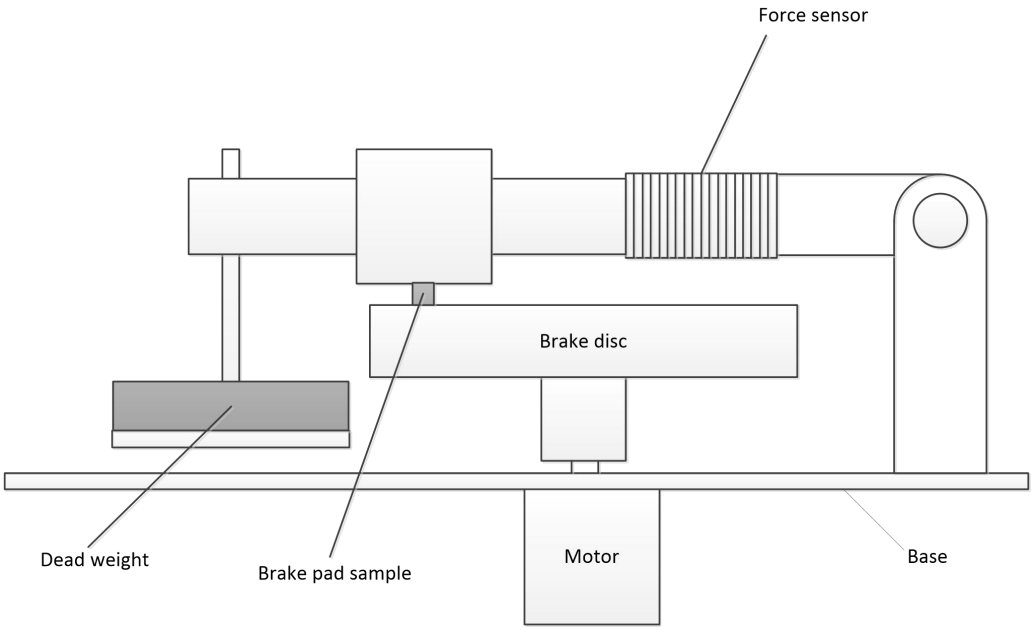

Figure 1. Schematic of tribometer

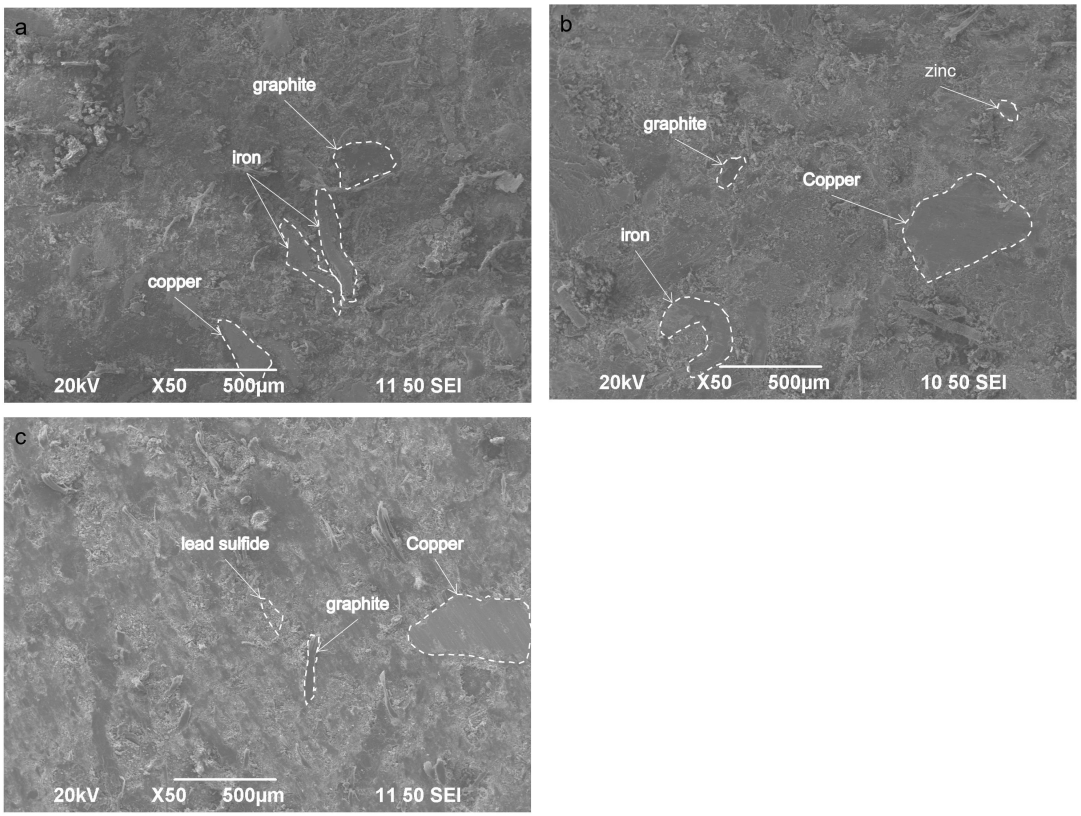

Figure 2. SEM pictures of brake pad samples. Some components are indicated. (a: SM brake pad, b: LM brake pad, c: NAO brake pad)

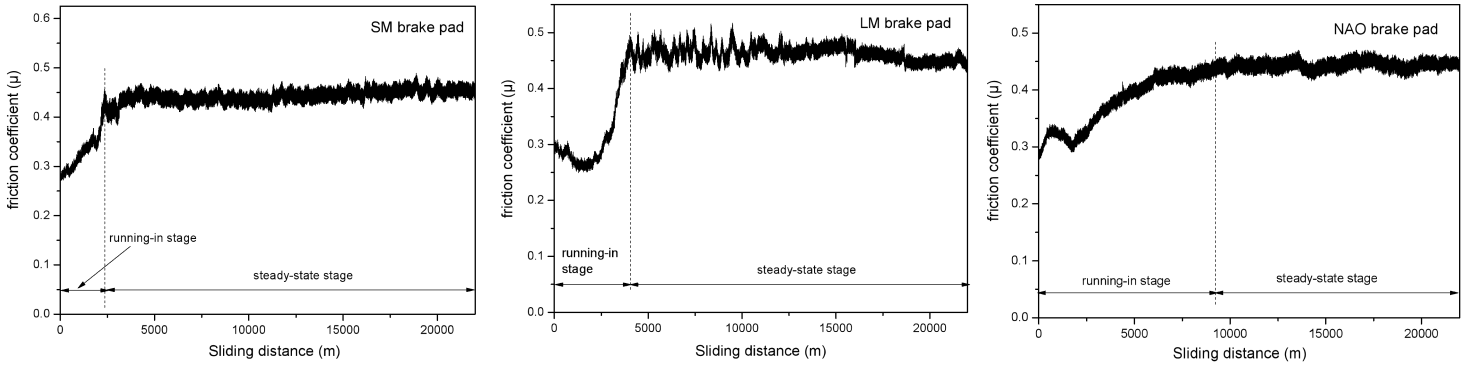

(A) Variation of friction coefficient during test (Test mode 2)

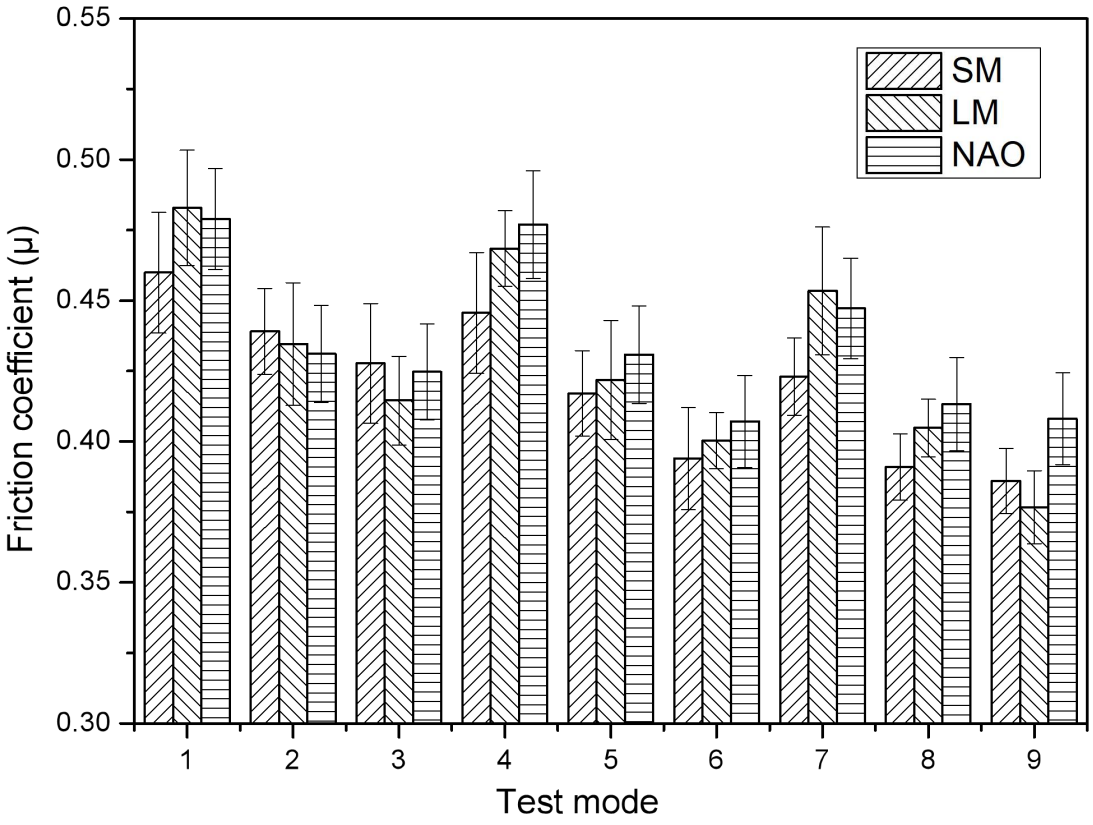

(B) Average friction coefficients at steady-state stage

Fig. 3. Friction coefficients of SM, LM and NAO brake pads sliding against iron disc

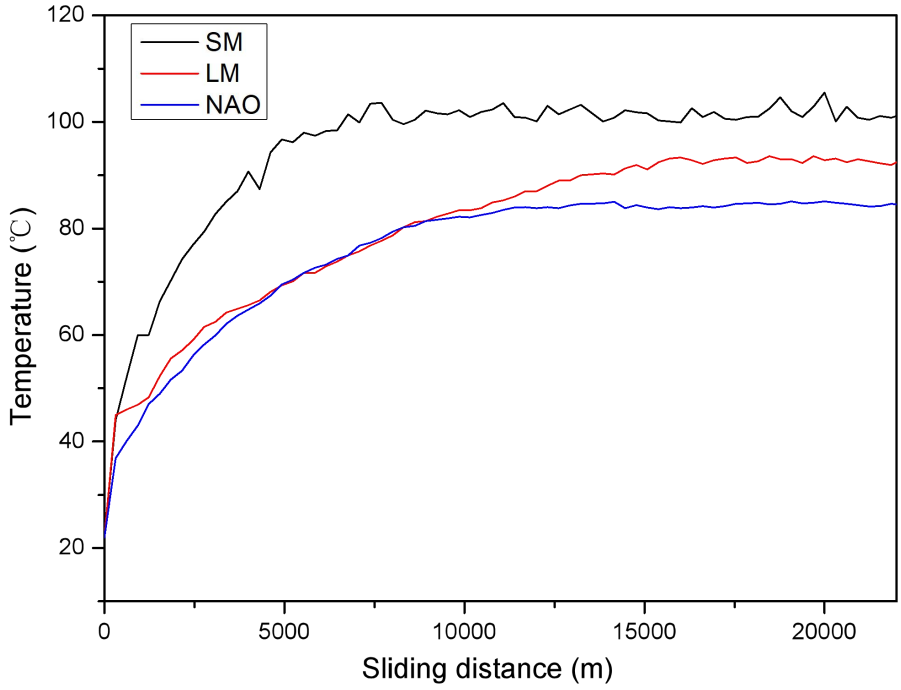

(A) Variation of contact temperature with sliding distance (Test mode 6)

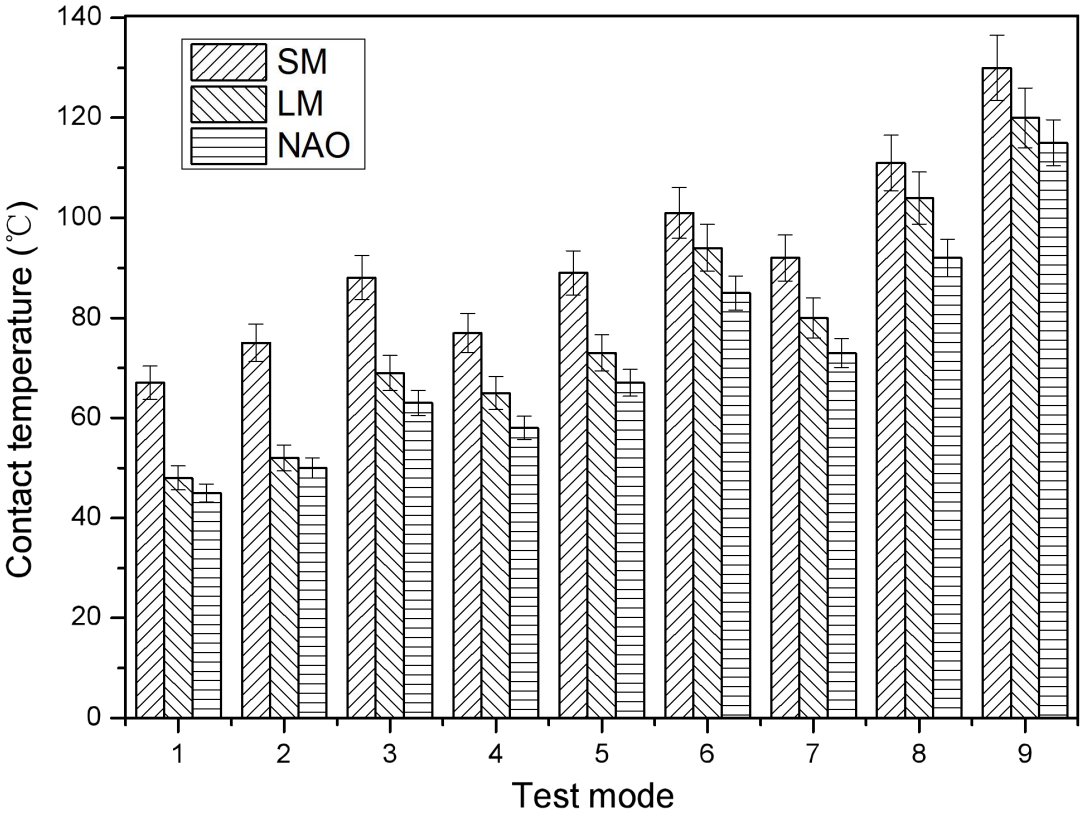

(B) Average contact temperatures at steady-state stage

Fig. 4. Contact temperatures of SM, LM and NAO brake pads sliding against iron disc

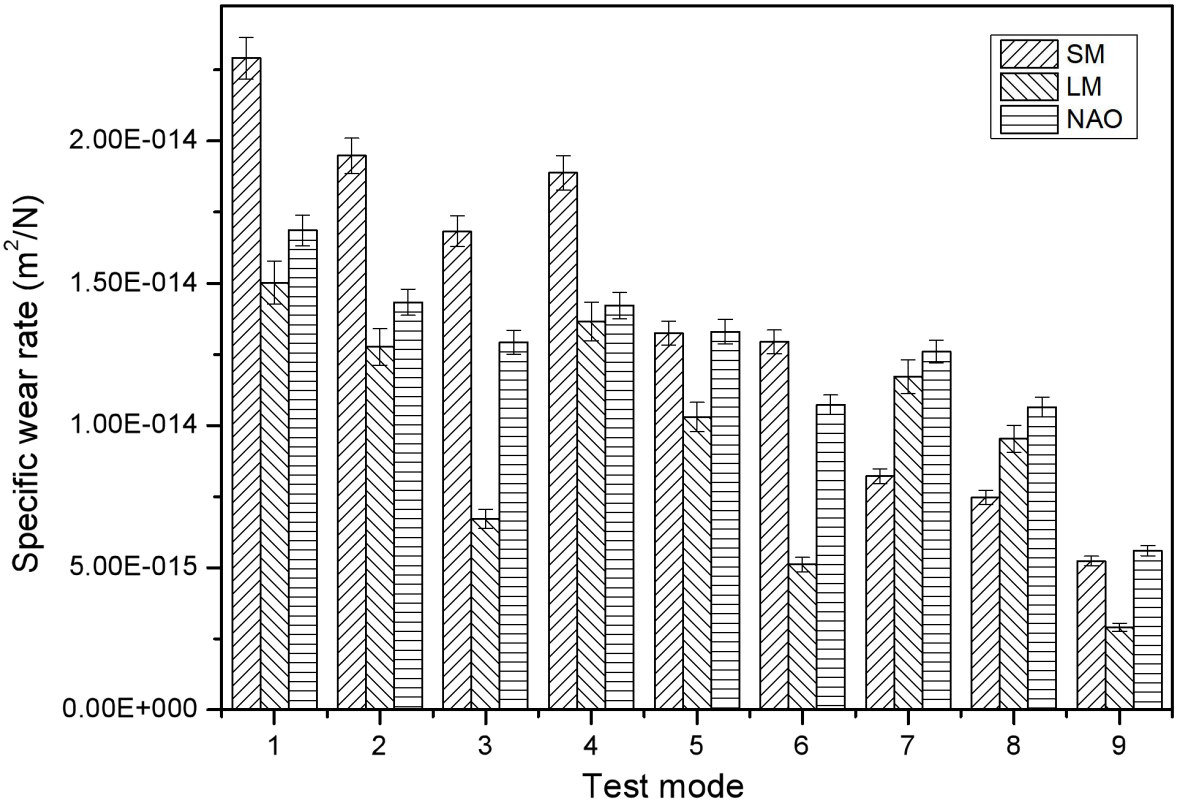

Fig. 5. Specific wear rates of SM, LM and NAO brake pads sliding against iron disc

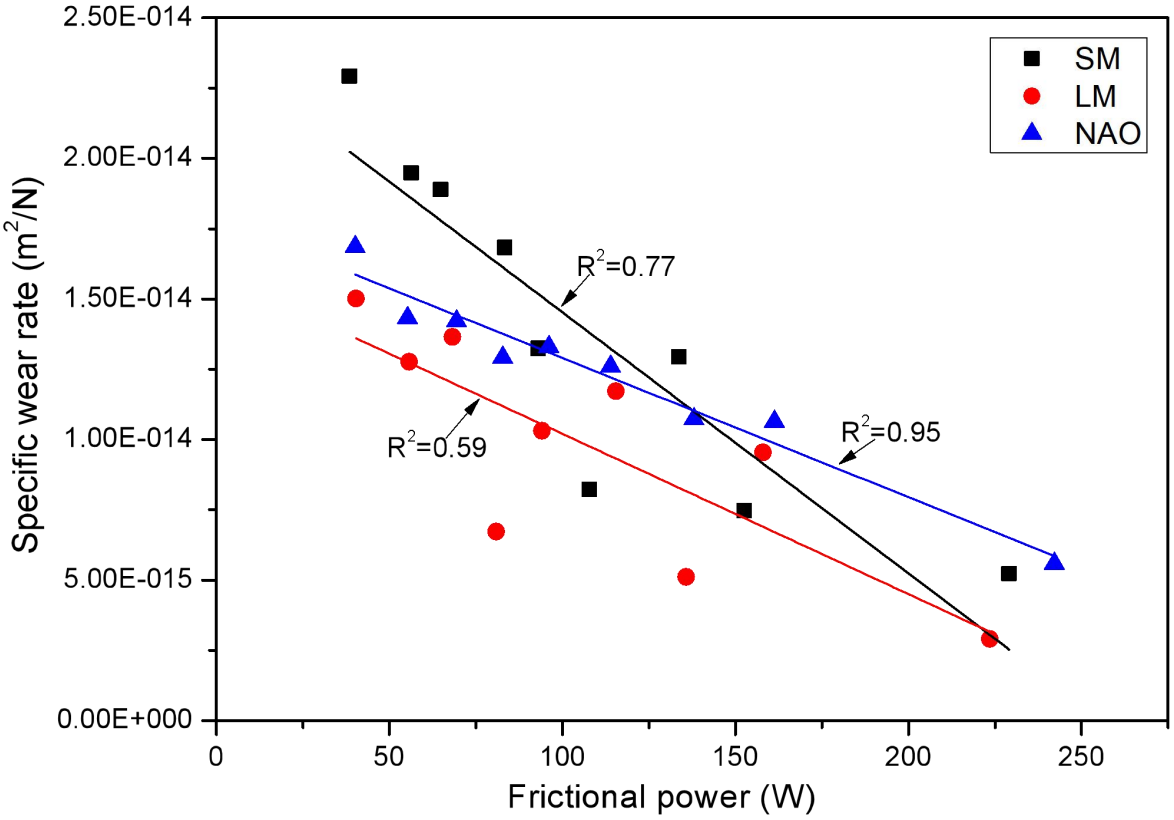

Fig. 6. Relationship between specific wear rate and frictional power

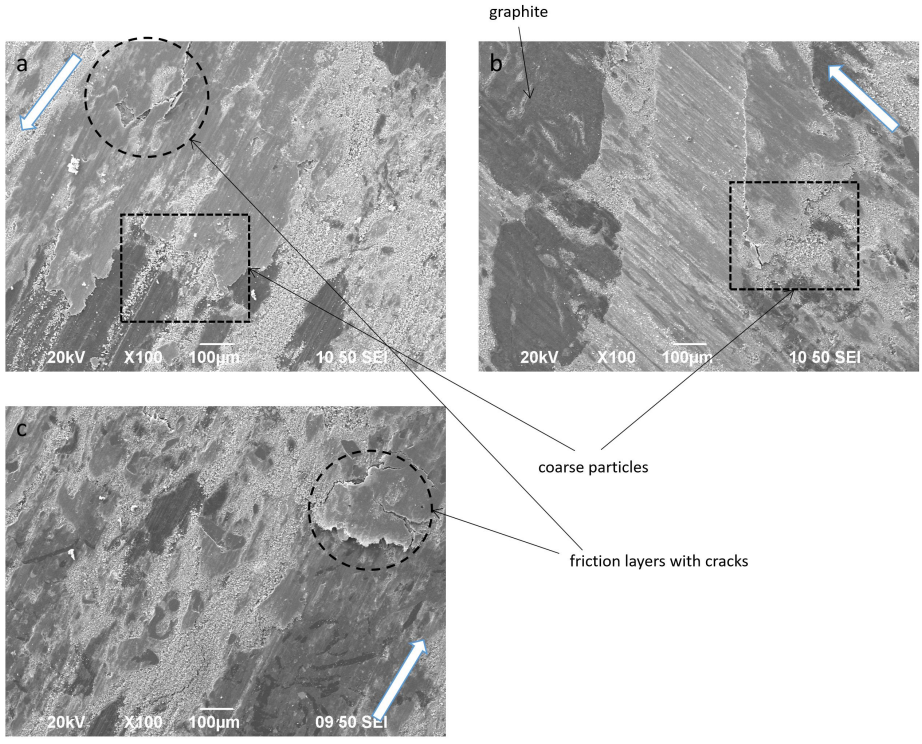

Fig. 7. SEM pictures of brake pad surfaces after mode 4 test (a: SM brake pad, b: LM brake pad, c: NAO brake pad; white arrow indicating the sliding direction)

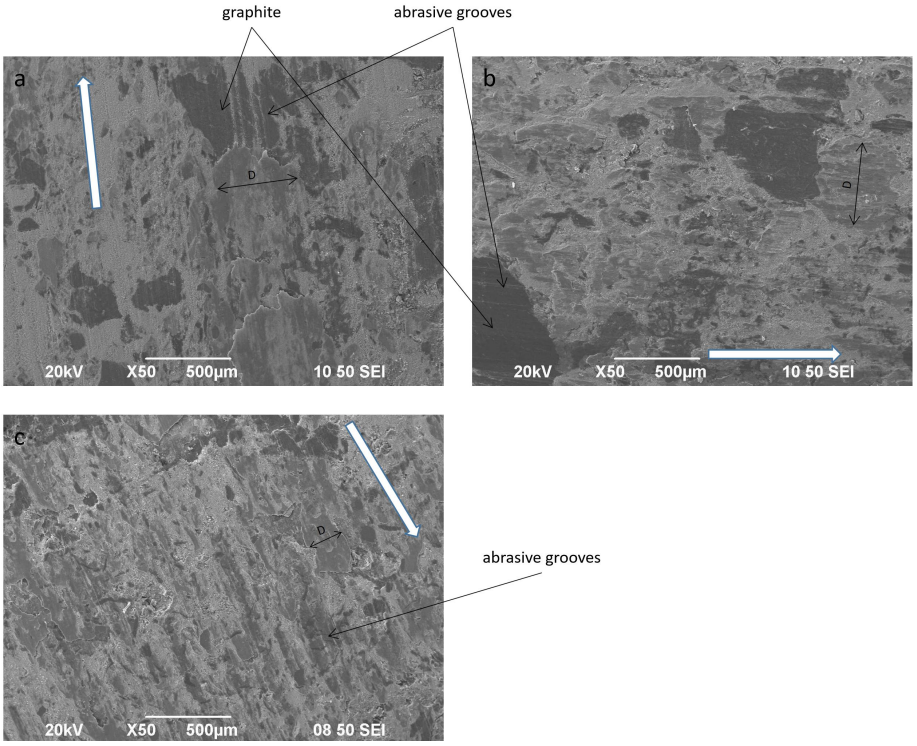

Fig. 8. SEM pictures of brake pad surfaces after mode 6 test (a: SM brake pad, b: LM brake pad, c: NAO brake pad; white arrow indicating the sliding direction)

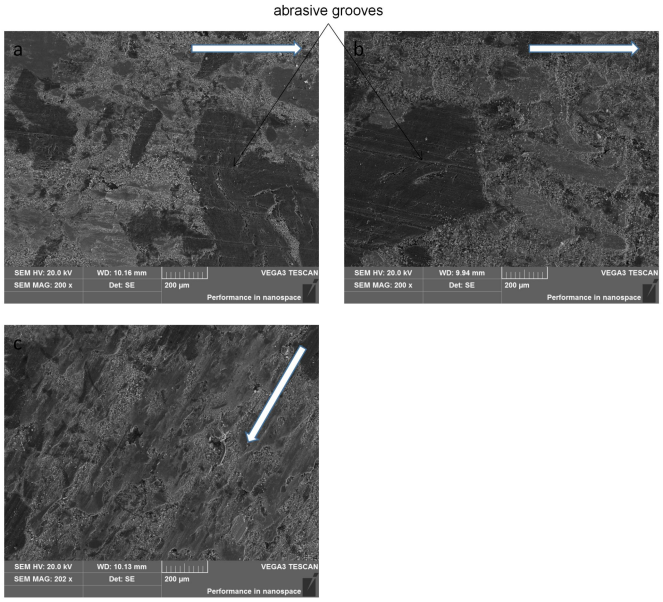

Fig. 9. SEM pictures of brake pad surfaces after mode 7 test (a: SM brake pad, b: LM brake pad, c: NAO brake pad; white arrow indicating the sliding direction)

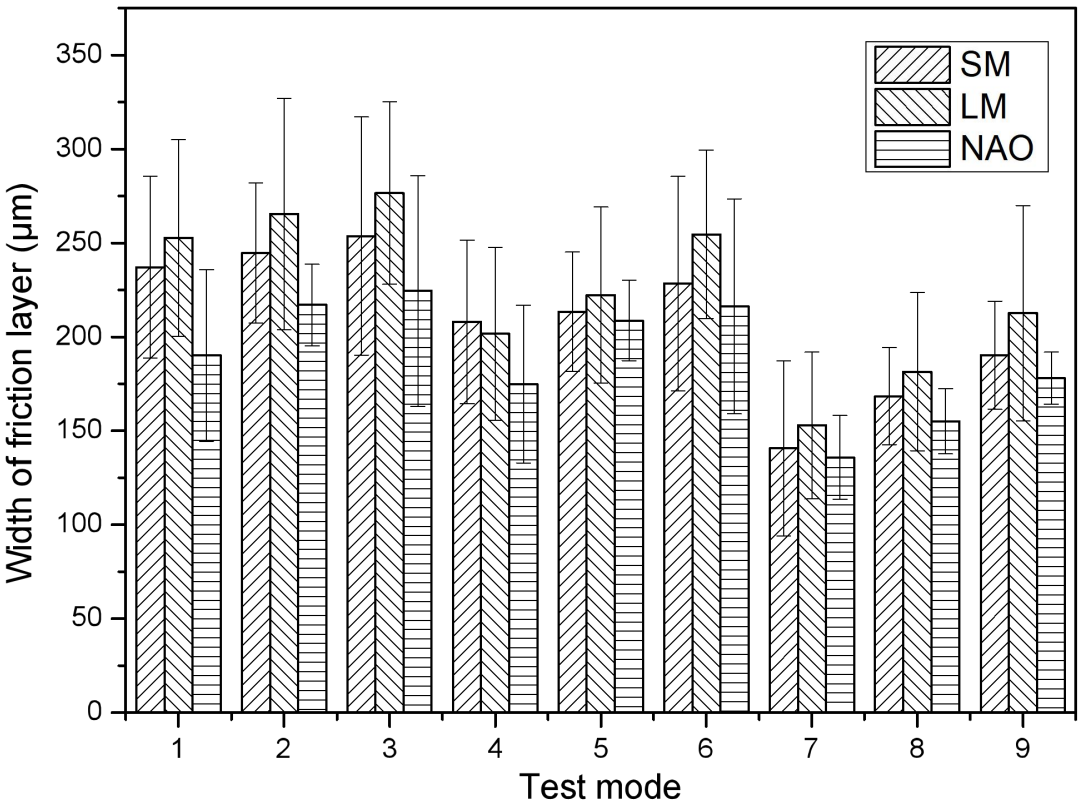

Fig. 10. Widths of friction layers on brake pad surfaces

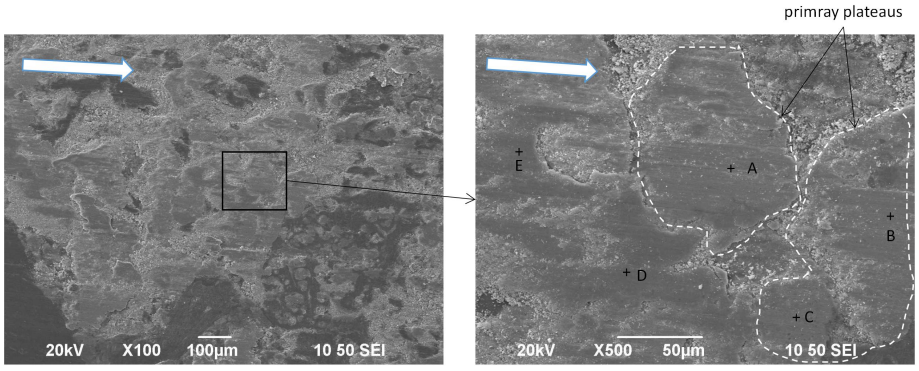

Spectrum: A

Element	Weight%	Atomic%
C K	9.89	33.79
Fe K	90.11	66.21
Totals	100.00	

Spectrum: B

Element	Weight%	Atomic%
C K	6.03	22.99
Fe K	93.97	77.01
Totals	100.00	

Spectrum: C

Element	Weight%	Atomic%
C K	6.35	23.98
Mn K	1.13	0.93
Fe K	92.52	75.09
Totals	100.00	

Spectrum: D

Element	Weight%	Atomic%
C K	9.92	25.69
O K	17.12	33.28
Si K	1.44	1.59
Ca K	2.46	1.91
Fe K	65.96	36.73
Sb L	3.10	0.79
Totals	100.00	

Spectrum: E

Element	Weight%	Atomic%
C K	9.07	23.39
O K	19.04	36.84
Si K	1.90	2.10
Ca K	2.43	1.88
Fe K	62.07	34.41
Sb L	5.49	1.39
Totals	100.00	

(a) LM brake pads

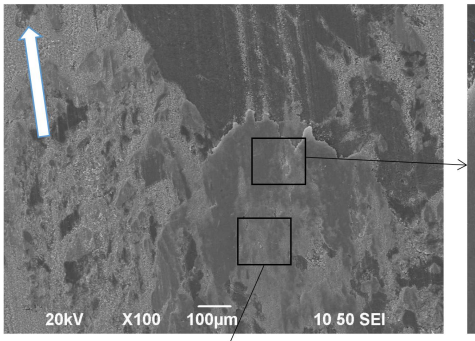

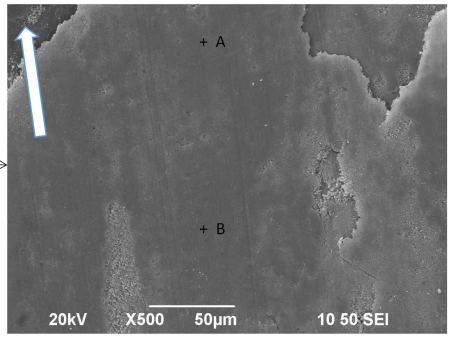

Spectrum: A

Element	Weight%	Atomic%
O K	13.44	35.28
Si K	2.22	3.32
Ca K	2.44	2.56
Fe K	72.65	54.63
Cu K	3.26	2.15
Sb L	5.98	2.06
Totals	100.00	

Spectrum: B

Element	Weight%	Atomic%
O K	13.50	35.19
Si K	2.60	3.87
Ca K	2.68	2.79
Mn K	1.34	1.01
Fe K	71.07	53.06
Cu K	3.38	2.22
Sb L	5.43	1.86
Totals	100.00	

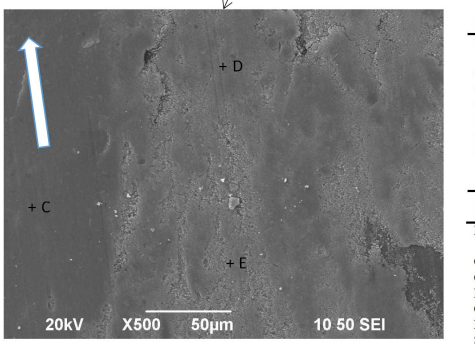

Spectrum: D

Element	Weight%	Atomic%
O K	14.95	37.92
Si K	2.27	3.28
Ca K	2.24	2.27
Fe K	72.66	52.80
Cu K	3.64	2.33
Sb L	4.24	1.41
Totals	100.00	

Spectrum: E

Element	Weight%	Atomic%
O K	14.41	37.95
Ca K	2.26	2.38
Fe K	70.40	53.12
Cu K	4.29	2.84
Rb L	4.84	2.39
Sb L	3.80	1.32
Totals	100.00	

Spectrum: C

Element	Weight%	Atomic%
O K	13.79	35.91
Si K	2.20	3.26
Ca K	2.94	3.05
Fe K	71.05	52.98
Cu K	4.36	2.86
Sb L	5.66	1.94
Totals	100.00	

(b) SM brake pads

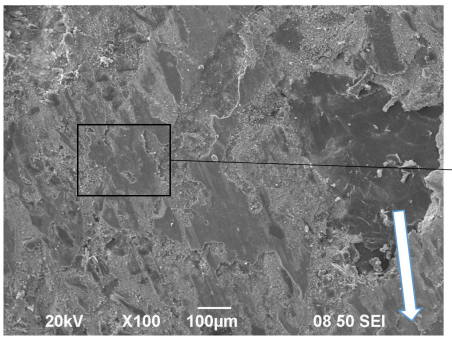

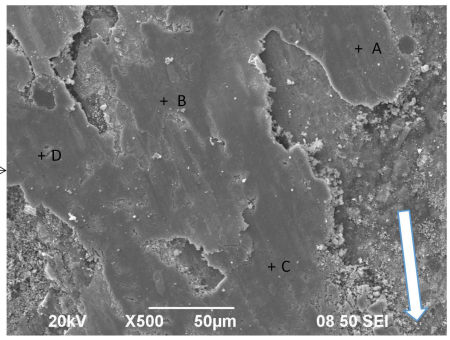

Spectrum: A

Element	Weight%	Atomic%
O K	9.80	27.02
Si K	3.22	5.06
Ca K	8.37	9.22
Ti K	1.31	1.20
Fe K	60.23	47.58
Cu K	7.29	5.06
Zn K	4.20	2.83
Sb L	5.59	2.02
Totals	100.00	

Spectrum: B

Element	Weight%	Atomic%
O K	18.03	41.49
Al K	1.02	1.39
Si K	4.32	5.67
K K	1.13	1.06
Ca K	6.29	5.78
Fe K	57.46	37.87
Cu K	7.66	4.44
Zn K	4.09	2.30
Totals	100.00	

Spectrum: C

Element	Weight%	Atomic%
O K	19.38	43.91
Si K	3.36	4.34
K K	0.93	0.87
Ca K	7.99	7.22
Ti K	1.27	0.96
Fe K	56.95	36.97
Cu K	6.77	3.86
Zn K	3.35	1.86
Totals	100.00	

Spectrum: D

Element	Weight%	Atomic%
C K	12.28	29.42
O K	17.88	32.17
Al K	0.88	0.94
Si K	3.20	3.28
Ca K	6.44	4.62
Ti K	1.13	0.68
Fe K	52.18	26.89
Cu K	2.66	1.21
Sb L	3.35	0.79
Totals	100.00	

(c) NAO brake pads

Fig. 11. SEM pictures and EDXS point spectra of the LM, SM and NAO brake pad surfaces (Test mode 6)

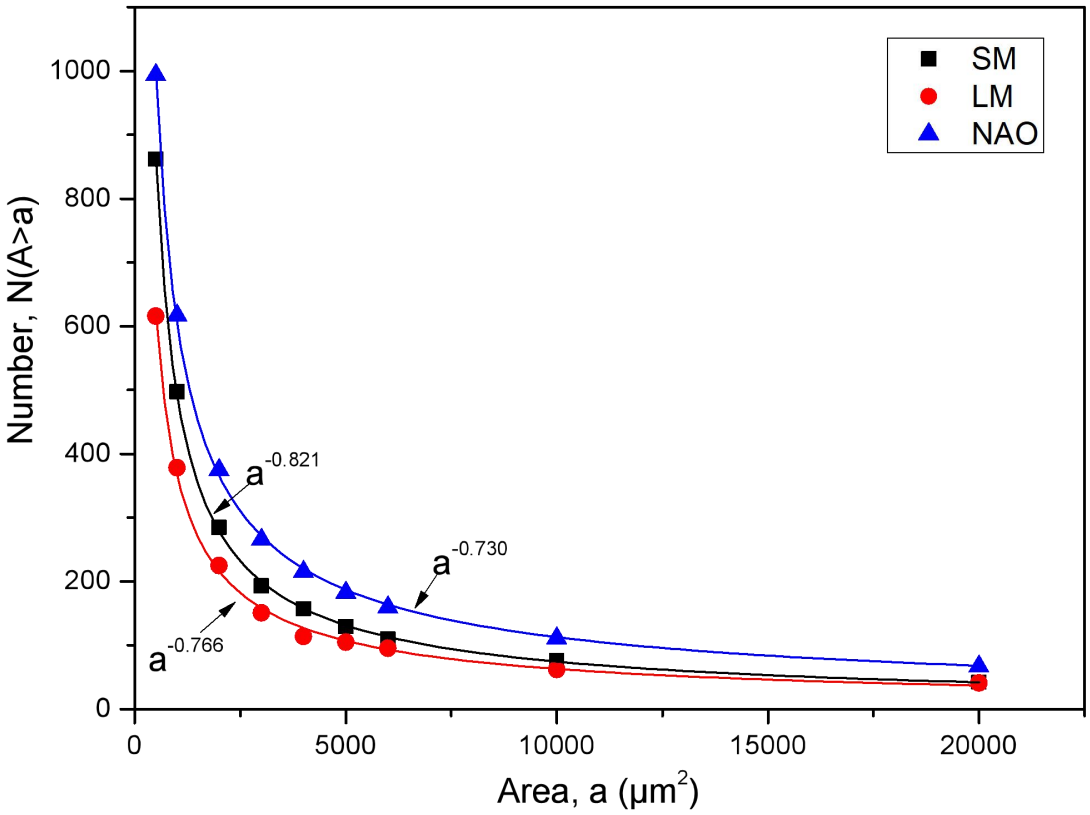

Fig. 12. Number-area distributions of contact plateaus on the brake pad surface (Test mode 4)

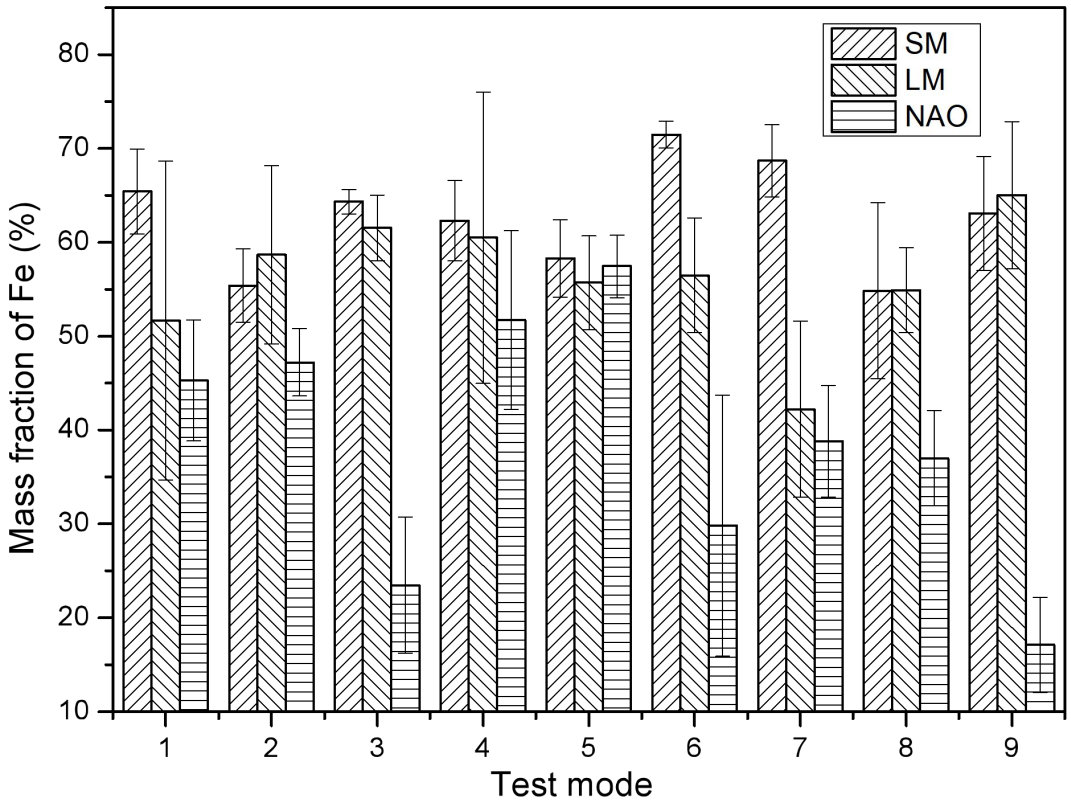

(a) Fe

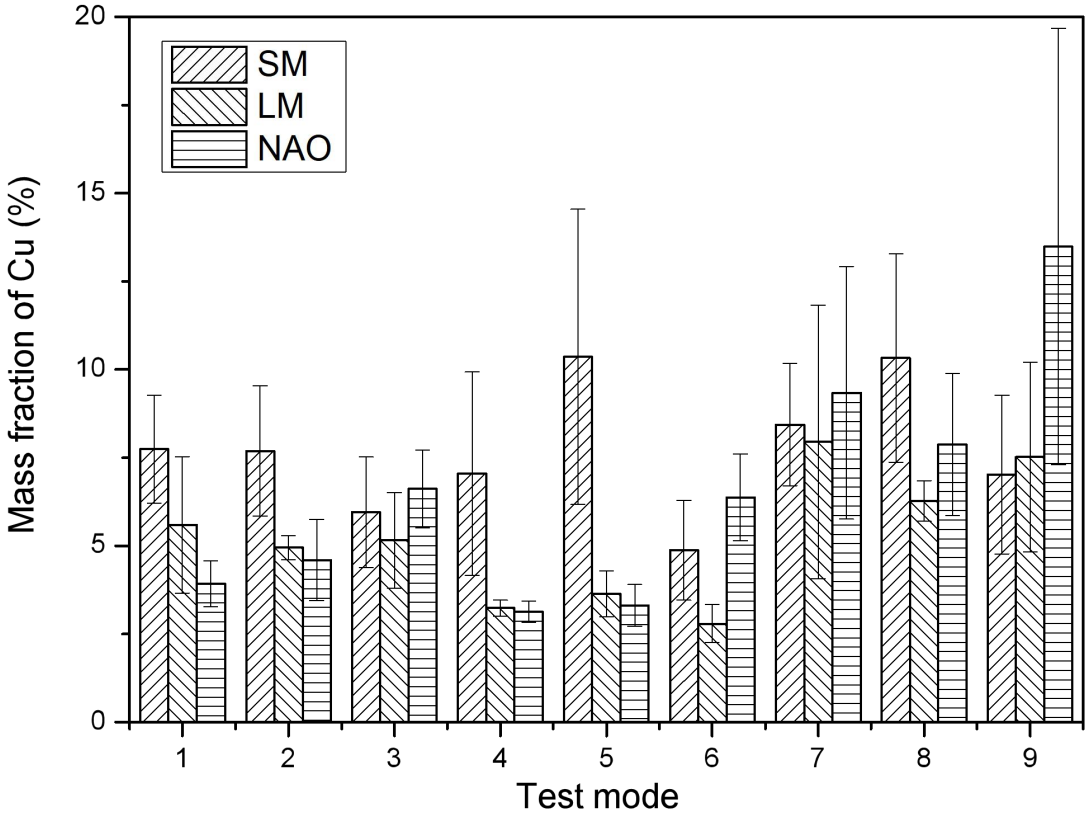

(b) Cu

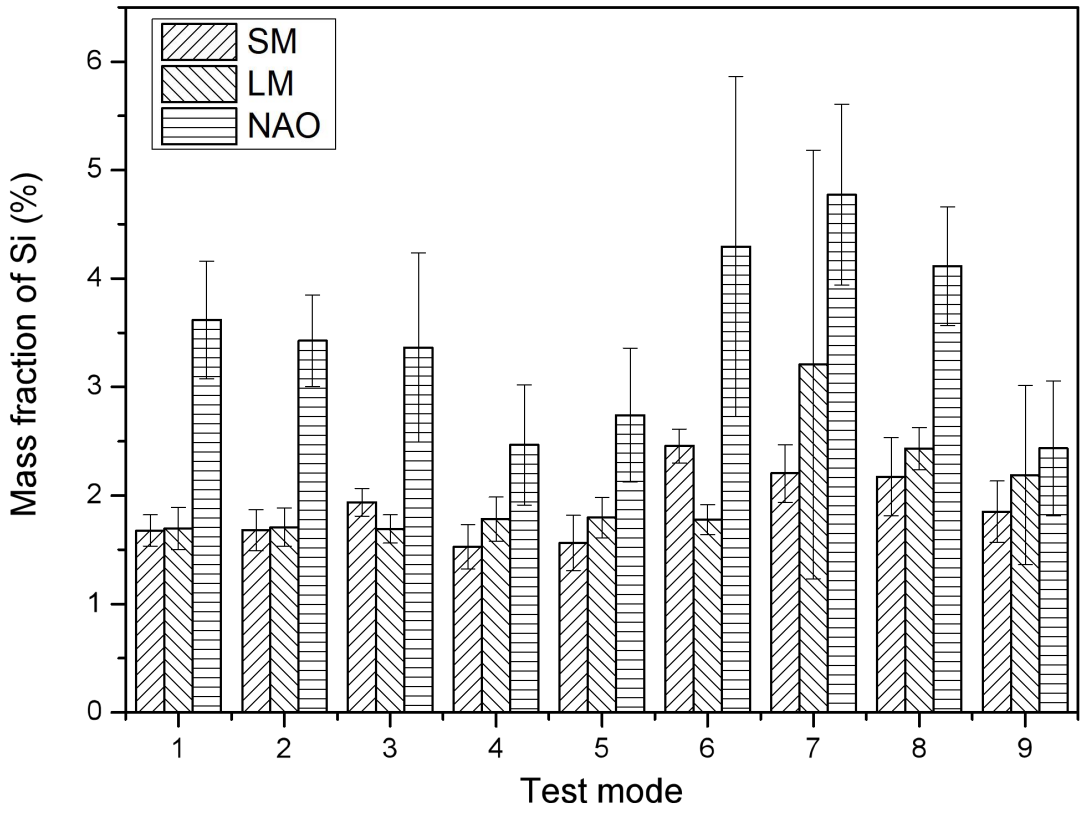

(c) Si

Fig. 13. Average mass fractions for selected elements measured on friction layers

A study of brake contact pairs under different friction conditions with respect to characteristics of brake pad surfaces

L. Wei, Y.S. Choy*, C.S. Cheung
Department of Mechanical Engineering, The Hong Kong Polytechnic University, Hung Hom, Kowloon, Hong Kong

*Corresponding author.
Tel: +852 2766 7813
Email: mmyschoy@polyu.edu.hk

Tables

Table 1. Element compositions and densities of brake pads

Element	SM brake pad (wt%)	LM brake pad (wt%)	NAO brake pad (wt%)
Mg	0.68	0.80	0.77
Al	1.10	1.38	4.16
Si	2.89	3.90	6.28
P	0.05	0.05	0.08
S	4.62	5.02	1.28
Cl	0.11	0.13	0.02
K	0.27	0.21	3.14
Ca	10.08	9.34	25.57
Ti	0.21	0.10	3.69
Cr	0.05	0.03	-
Mn	0.15	0.20	0.08
Fe	34.38	25.94	13.42
Ni	0.04	0.06	-
Cu	4.09	5.67	1.55
Zn	0.75	1.37	1.06
As	-	-	0.44
Se	0.02	-	-
Sr	0.02	-	0.03
Zr	0.03	-	-

Mo	0.01	-	-
Sb	7.41	6.94	4.01
Pb	0.31	0.22	-
Densities (g/cm^3)	2.76±0.04	2.75±0.12	2.12±0.07

Table 2. Test conditions and fractal dimensions

Test mode	Sliding velocity (m/s)	Nominal contact pressure (MPa)	Frictional power (W)			Fractal dimension (D_s)		
			SM	LM	NAO	SM	LM	NAO
1	1.6	0.52	38.50	40.42	40.10	2.56	2.62	2.53
2	1.6	0.81	56.30	55.72	55.28	2.67	2.61	2.46
3	1.6	1.22	83.41	80.84	82.83	2.59	2.49	2.53
4	2.8	0.52	64.87	68.19	69.43	2.64	2.53	2.46
5	2.8	0.81	93.01	94.08	96.07	2.51	2.52	2.46
6	2.8	1.22	133.61	135.79	138.07	2.42	2.38	2.48
7	4.9	0.52	107.77	115.51	113.92	2.47	2.71	2.59
8	4.9	0.81	152.60	157.98	161.30	2.84	2.71	2.45
9	4.9	1.22	229.11	223.56	242.21	2.76	2.60	2.59

Table 3. Main phase compositions (wt%) of the friction layers on brake pad surface

(a) SM brake pad

	1.6m/s			2.8m/s			4.9m/s		
	0.52MPa	0.81MPa	1.22MPa	0.52MPa	0.81MPa	1.22MPa	0.52MPa	0.81MPa	1.22MPa
Graphite	55.6	43.4	39.5	50.7	41.9	38.2	60.5	37.0	48.6
Copper	12.3	11.2	11.5	13.7	11.3	12.8	10.8	11.6	9.6
Hematite (Fe_2O_3)	11.2	18.9	17.6	10.1	22.6	23.4	12.4	12.6	14.4
Calcite ($CaCO_3$)	15.9	18.5	25.3	21.1	19.6	20.6	10.7	30.9	16.3
Stibnite (Sb_2S_3)	4.8	8.0	6.2	4.3	4.5	5.0	5.3	7.9	11.0

(b) LM brake pad

	1.6m/s			2.8m/s			4.9m/s		
	0.52MPa	0.81MPa	1.22MPa	0.52MPa	0.81MPa	1.22MPa	0.52MPa	0.81MPa	1.22MPa
Graphite	62.1	47.4	46.8	47.9	64.1	49.7	46.9	60.0	43.9
Copper	4.6	12.9	16.9	15.3	1.5	24.7	10.5	7.6	9.1
Hematite (Fe_2O_3)	12.1	13.5	12.3	16.8	10.5	10.5	10.2	13.6	14.0

Calcite ($CaCO_3$)	15.7	22.0	17.5	19.6	19.2	12.5	24.3	12.1	22.4
Stibnite (Sb_2S_3)	4.9	4.3	6.8	0.3	3.0	2.4	8.2	6.7	11.2

(c) NAO brake pad

	1.6m/s			2.8m/s			4.9m/s		
	0.52MPa	0.81MPa	1.22MPa	0.52MPa	0.81MPa	1.22MPa	0.52MPa	0.81MPa	1.22MPa
Graphite	38.4	45.3	34.3	41.4	34.1	53.4	35.4	34.4	37.2
Copper	10.1	5.6	0.8	9.3	1.1	10.3	10.9	0.5	0.8
Hematite (Fe_2O_3)	9.3	6.8	10.9	9.6	9.7	3.8	9.0	12.0	9.8
Calcite ($CaCO_3$)	41.5	42.2	52.4	39.7	52.8	32.6	43.2	51.9	51.7
Stibnite (Sb_2S_3)	0.3	0.8	1.9	0.3	2.0	0.4	0.2	1.7	1.1

A study of brake contact pairs under different friction conditions with respect to characteristics of brake pad surfaces

L. Wei, Y.S. Choy*, C.S. Cheung
Department of Mechanical Engineering, The Hong Kong Polytechnic University, Hung Hom, Kowloon, Hong Kong

*Corresponding author.
Tel: +852 2766 7813
Email: mmyschoy@polyu.edu.hk

Supplementary information

Figures

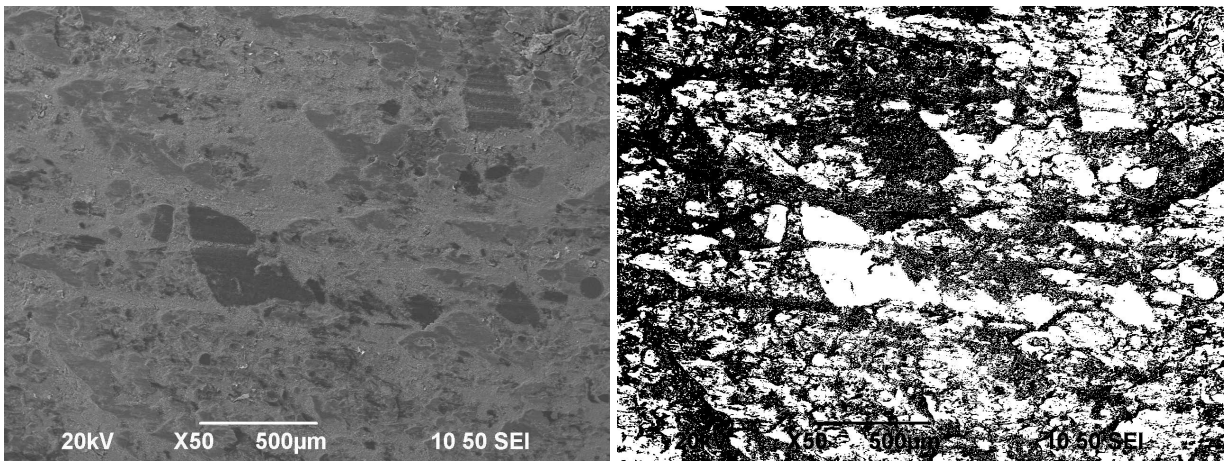

Fig. S1. SEM pictures before (left) and after (right) segmentation process (Test mode 6)

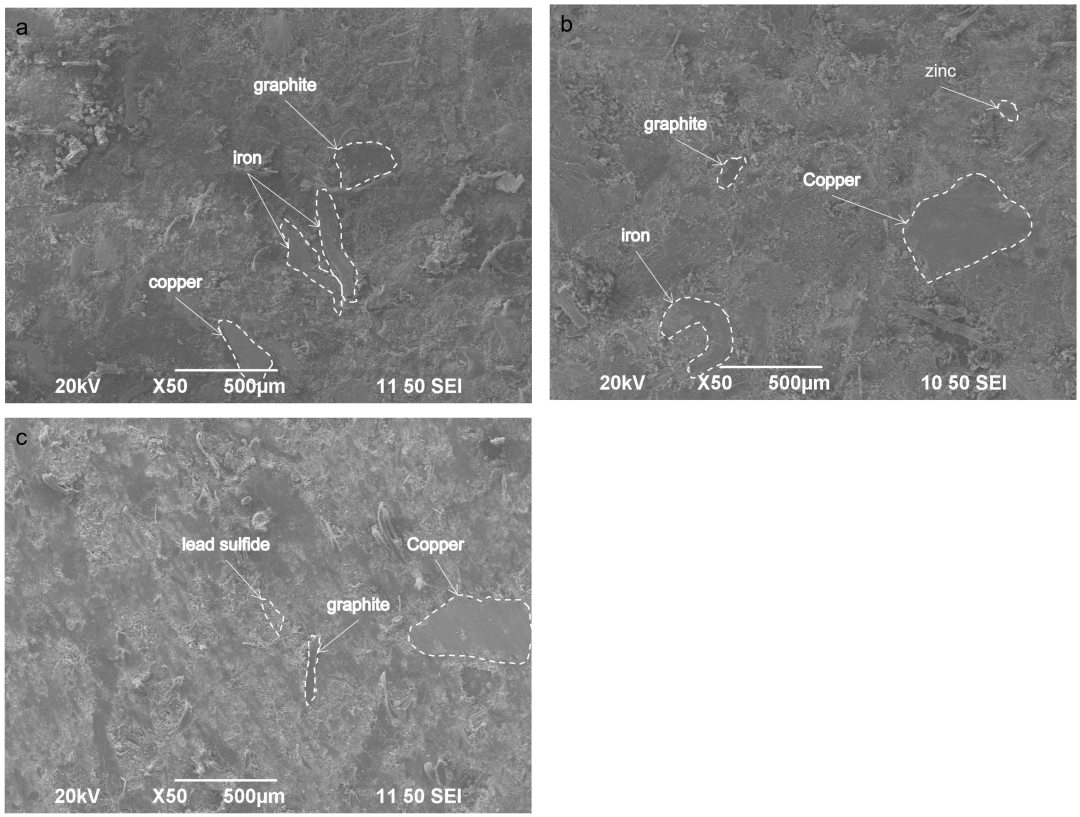

Fig. S2. SEM pictures of brake pad samples. Some components are indicated by EDXS point spectra. (a: SM brake pad, b: LM brake pad, c: NAO brake pad)

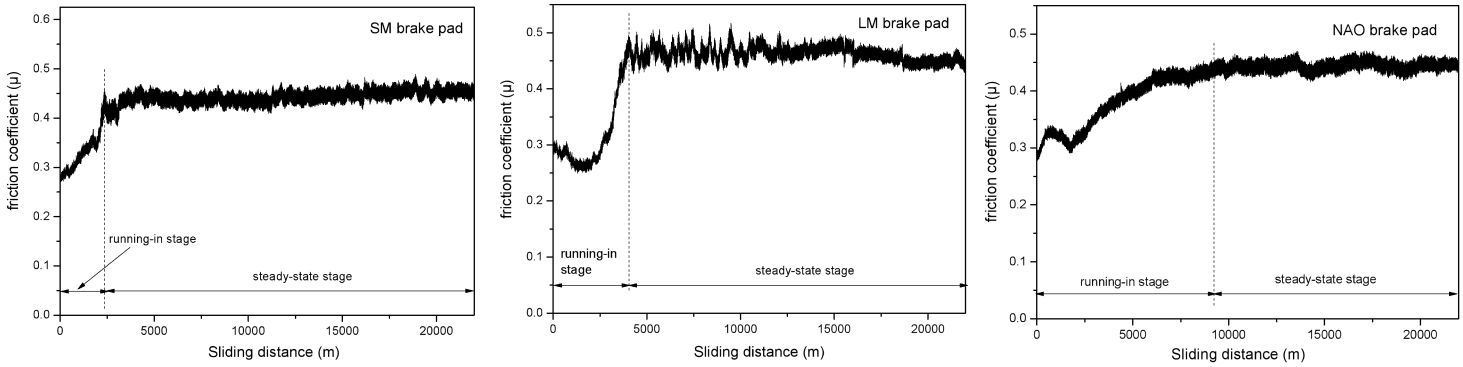

Fig. S3. Variation of friction coefficient during test (Test mode 2)

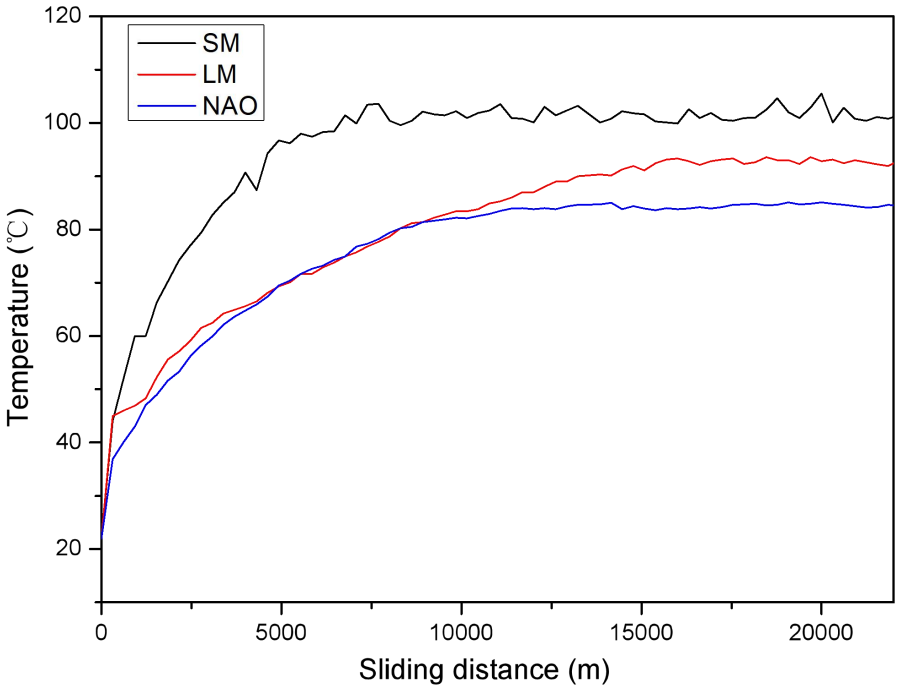

Fig. S4. Variation of brake pad temperature with sliding distance (Test mode 6)

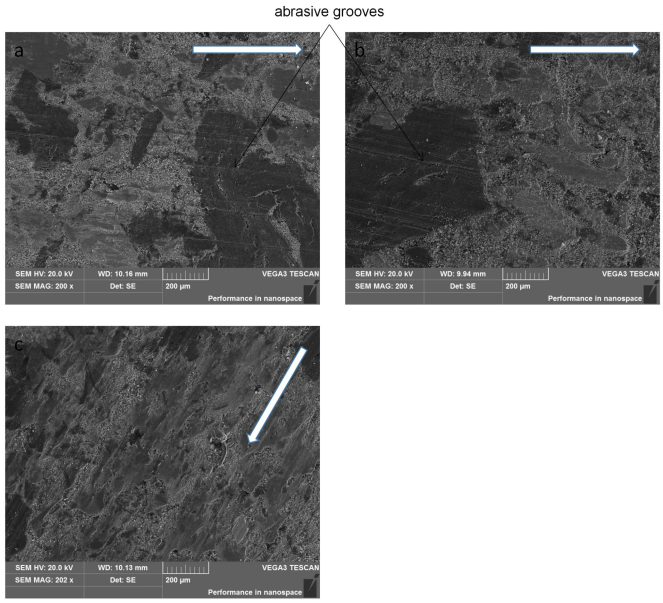

Fig. S5. SEM pictures of brake pad surfaces after mode 7 test (a: SM brake pad, b: LM brake pad, c: NAO brake pad; white arrow indicating the sliding direction)

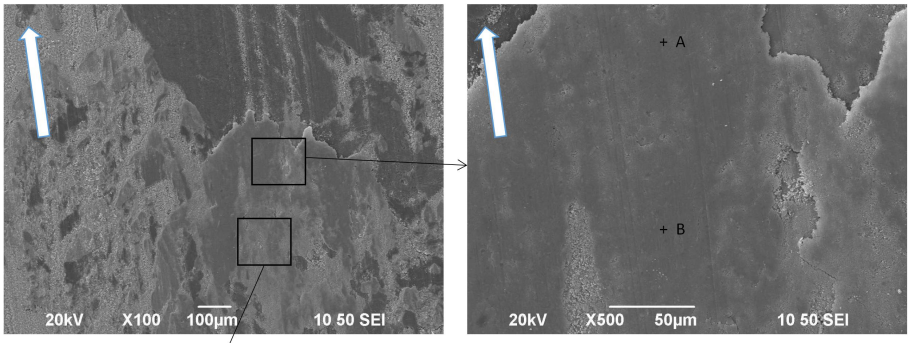

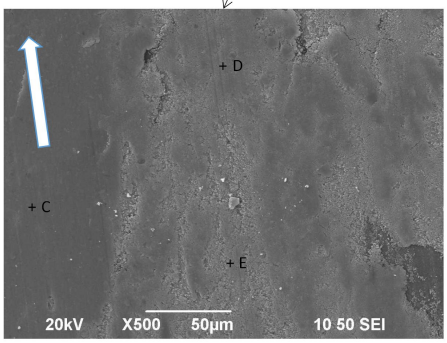

Spectrum: A

Element	Weight%	Atomic%
O K	13.44	35.28
Si K	2.22	3.32
Ca K	2.44	2.56
Fe K	72.65	54.63
Cu K	3.26	2.15
Sb L	5.98	2.06
Totals	100.00	

Spectrum: B

Element	Weight%	Atomic%
O K	13.50	35.19
Si K	2.60	3.87
Ca K	2.68	2.79
Mn K	1.34	1.01
Fe K	71.07	53.06
Cu K	3.38	2.22
Sb L	5.43	1.86
Totals	100.00	

Spectrum: C

Element	Weight%	Atomic%
O K	13.79	35.91
Si K	2.20	3.26
Ca K	2.94	3.05
Fe K	71.05	52.98
Cu K	4.36	2.86
Sb L	5.66	1.94
Totals	100.00	

Spectrum: D

Element	Weight%	Atomic%
O K	14.95	37.92
Si K	2.27	3.28
Ca K	2.24	2.27
Fe K	72.66	52.80
Cu K	3.64	2.33
Sb L	4.24	1.41
Totals	100.00	

Spectrum: E

Element	Weight%	Atomic%
O K	14.41	37.95
Ca K	2.26	2.38
Fe K	70.40	53.12
Cu K	4.29	2.84
Rb L	4.84	2.39
Sb L	3.80	1.32
Totals	100.00	

(a) SM brake pads

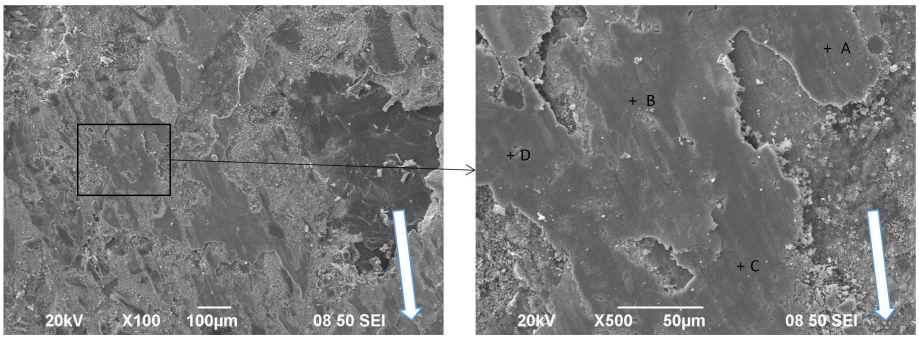

Spectrum: A

Element	Weight%	Atomic%
O K	9.80	27.02
Si K	3.22	5.06
Ca K	8.37	9.22
Ti K	1.31	1.20
Fe K	60.23	47.58
Cu K	7.29	5.06
Zn K	4.20	2.83
Sb L	5.59	2.02
Totals	100.00	

Spectrum: B

Element	Weight%	Atomic%
O K	18.03	41.49
Al K	1.02	1.39
Si K	4.32	5.67
K K	1.13	1.06
Ca K	6.29	5.78
Fe K	57.46	37.87
Cu K	7.66	4.44
Zn K	4.09	2.30
Totals	100.00	

Spectrum: C

Element	Weight%	Atomic%
O K	19.38	43.91
Si K	3.36	4.34
K K	0.93	0.87
Ca K	7.99	7.22
Ti K	1.27	0.96
Fe K	56.95	36.97
Cu K	6.77	3.86
Zn K	3.35	1.86
Totals	100.00	

Spectrum: D

Element	Weight%	Atomic%
C K	12.28	29.42
O K	17.88	32.17
Al K	0.88	0.94
Si K	3.20	3.28
Ca K	6.44	4.62
Ti K	1.13	0.68
Fe K	52.18	26.89
Cu K	2.66	1.21
Sb L	3.35	0.79
Totals	100.00	

(b) NAO brake pads

Fig. S6. SEM pictures and EDXS point spectra of SM and NAO brake pad surface (Test mode 6)

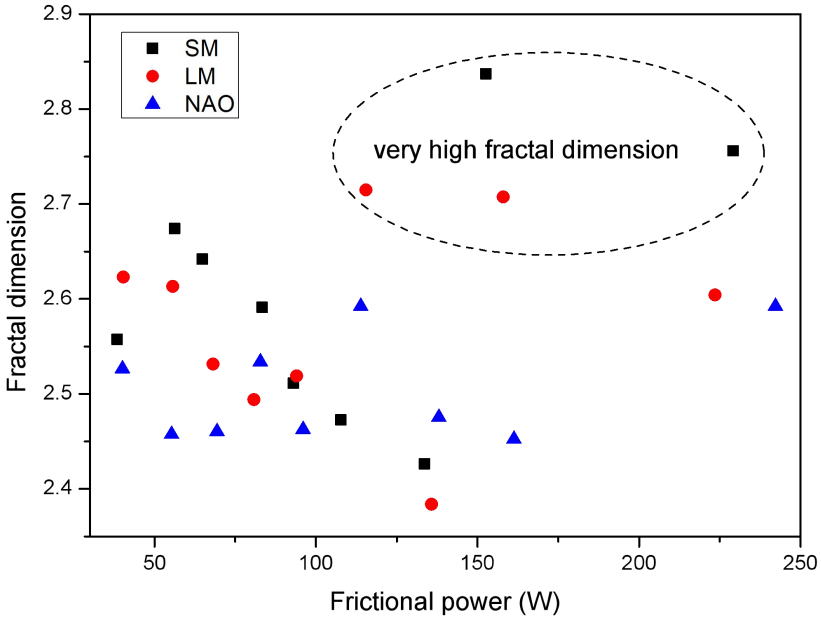

Fig. S7. The variation fractal dimension versus frictional power

Tables

Table S1. 3^2 ANOVA results for friction coefficient

(a) SM brake pad

Source	Sum of squares	Degrees of freedom	Mean square	F	P-value
Sliding velocity	0.00804	2	0.00402	17.66	<0.01
Contact pressure	0.00759	2	0.00380	16.67	<0.01
Interaction	<0.001	4	<0.001	0.48	0.75
Error	0.00408	18	<0.001		
Total	0.0201	26			

(b) LM brake pad

Source	Sum of squares	Degrees of freedom	Mean square	F	P-value
Sliding velocity	0.00474	2	0.00237	13.22	<0.01
Contact pressure	0.0236	2	0.0118	65.80	<0.01
Interaction	<0.001	4	<0.001	0.13	0.97
Error	0.00323	18	<0.001		
Total	0.0317	26			

(c) NAO brake pad

Source	Sum of squares	Degrees of freedom	Mean square	F	P-value
Sliding velocity	0.00231	2	0.00116	6.33	<0.01
Contact pressure	0.0147	2	0.00737	40.41	<0.01
Interaction	<0.001	4	<0.001	1.10	0.39
Error	0.00328	18	<0.001		
Total	0.0211	26			

Table S2. 3^2 ANOVA results for contact temperature

(a) SM brake pad

Source	Sum of squares	Degrees of freedom	Mean square	F	P-value
Sliding velocity	5445	2	2722	158	<0.01
Contact pressure	3449	2	1724	100	<0.01
Interaction	255	4	63	3.70	0.02
Error	311	18	17		
Total	9459	26			

(b) LM brake pad

Source	Sum of squares	Degrees of freedom	Mean square	F	P-value
Sliding velocity	9126	2	4563	352	<0.01
Contact pressure	4104	2	2052	158	<0.01
Interaction	420	4	105	8.10	<0.01
Error	233	18	13		
Total	13883	26			

(c) NAO brake pad

Source	Sum of squares	Degrees of freedom	Mean square	F	P-value
Sliding velocity	7496	2	3748	534	<0.01
Contact pressure	3858	2	1929	275	<0.01
Interaction	448	4	112	16	<0.01
Error	126	18	7		
Total	11928	26			

Table S3. 3^2 ANOVA results for specific wear rate

(a) SM brake pad

Source	Sum of squares	Degrees of freedom	Mean square	F	P-value
Sliding velocity	7.51E-28	2	3.75E-28	2072	<0.01
Contact pressure	1.17E-28	2	5.83E-29	321	<0.01
Interaction	2.14E-29	4	5.35E-30	30	<0.01
Error	3.26E-30	18	1.81E-31		
Total	8.92E-28	26			

(b) LM brake pad

Source	Sum of squares	Degrees of freedom	Mean square	F	P-value
Sliding velocity	5.36E-29	2	2.68E-29	125	<0.01
Contact pressure	3.46E-28	2	1.73E-28	807	<0.01
Interaction	2.05E-30	4	5.12E-31	13	<0.01
Error	3.86E-30	18	2.14E-31		
Total	4.06E-28	26			

(c) NAO brake pad

Source	Sum of squares	Degrees of freedom	Mean square	F	P-value
Sliding velocity	1.19E-28	2	5.94E-29	460	<0.01
Contact pressure	1.06E-28	2	6.31E-28	411	<0.01
Interaction	1.56E-29	4	3.9E-30	30	<0.01
Error	2.33E-30	18	1.29E-31		
Total	2.43E-28	26			

Table S4. 3^2 ANOVA results for width of friction layer

(a) SM brake pad

Source	Sum of squares	Degrees of freedom	Mean square	F	P-value
Sliding velocity	285659	2	142829	9.36	<0.01
Contact pressure	33768	2	16884	1.11	0.33
Interaction	14183	4	3546	0.23	0.92
Error	3981951	261	15257		
Total	4315561	269			

(b) LM brake pad

Source	Sum of squares	Degrees of freedom	Mean square	F	P-value
Sliding velocity	306891	2	153445	8.12	<0.01
Contact pressure	76227	2	38113	2.02	0.14
Interaction	28426	4	7106	0.38	0.83
Error	4930488	261	18891		
Total	5342031	269			

(c) NAO brake pad

Source	Sum of squares	Degrees of freedom	Mean square	F	P-value
Sliding velocity	96312	2	48171	4.33	0.01
Contact pressure	65765	2	32883	2.96	0.05
Interaction	2250	4	563	0.05	0.99
Error	2903941	18	11126		
Total	3068299	26			

Table S5. Linear fitting parameters for the relationship between frictional power and specific wear rate

Type of brake pad	Slope	Intercept	Adj. R-Square
SM	-9.29E-17	2.38E-14	0.77
LM	-5.70E-17	1.59E-14	0.59
NAO	-4.95E-17	1.79E-14	0.95

Table S6. 3^2 ANOVA results for Fe content in secondary plateaus

(a) SM brake pad

Source	**Sum of squares**	**Degrees of freedom**	**Mean square**	**F**	**P-value**
Sliding velocity	89.5	2	44.7	0.72	0.49
Contact pressure	1891	2	946	15.27	<0.01
Interaction	593	4	148	2.39	0.057
Error	5018	81	61.9		
Total	7591	89			

(b) LM brake pad

Source	**Sum of squares**	**Degrees of freedom**	**Mean square**	**F**	**P-value**
Sliding velocity	230.2	2	115	0.46	0.63
Contact pressure	1373	2	687	2.75	0.07
Interaction	1893	4	473	1.90	0.12
Error	20208	81	249		
Total	23704	89			

(c) NAO brake pad

Source	**Sum of squares**	**Degrees of freedom**	**Mean square**	**F**	**P-value**
Sliding velocity	3533	2	1766	12.5	<0.01
Contact pressure	10422	2	5211	36.9	<0.01
Interaction	197	4	48.9	0.35	0.85
Error	11435	81	141		
Total	25587	89			

Table S7. 3^2 ANOVA results for Cu content in secondary plateaus

(a) SM brake pad

Source	Sum of squares	Degrees of freedom	Mean square	F	P-value
Sliding velocity	36	2	18.2	1.19	0.31
Contact pressure	185	2	92.4	6.04	<0.01
Interaction	44	4	10.9	0.71	0.59
Error	1240	81	15.3		
Total	1505	89			

(b) LM brake pad

Source	Sum of squares	Degrees of freedom	Mean square	F	P-value
Sliding velocity	243	2	122	14.48	<0.01
Contact pressure	6.36	2	3.18	0.38	0.66
Interaction	14.5	4	3.63	0.43	0.79
Error	680	81	8.40		
Total	944	89			

(c) NAO brake pad

Source	Sum of squares	Degrees of freedom	Mean square	F	P-value
Sliding velocity	631	2	316	18.2	<0.01
Contact pressure	240	2	120	6.91	<0.01
Interaction	35	4	8.67	0.50	0.74
Error	1408	81	17.4		
Total	2314	89			